LARGE SCALE TESTING OF MASONRY WALLS UNDER THE EFFECT OF REPRESENTATIVE GROUND SETTLEMENTS

A Thesis Submitted to
the Graduate School of Engineering and Sciences of
İzmir Institute of Technology
in Partial Fulfilment of the Requirements for Degree of

MASTER OF SCIENCE

in Civil Engineering

by
Berkay ÖZDEMİR

February 2022
İZMİR

ACKNOWLEDGMENTS

This study is a product of me and people who encouraged and supported me in all my hopeless times. In this part, I will express them gratitude towards one by one.

I would like to give special thanks to my special supervisor Dr. Korhan Deniz DALGIÇ who included me in this scientific study, guided me in every part of the study such as planning, research and execution, gave me insight in scientific terms with his experience. He never withheld his patience and understanding.

I would like to express my thanks to the jury members Assoc. Prof. Dr. İzzet ÖZDEMİR and Assoc. Prof. Dr. Sinan AÇIKGÖZ for participating in the thesis defense seminar and sharing their valuable suggestions for this study.

Special thanks to my teammates MSc. Burcu GÜLEN and MSc. Yiyan LIU for their support in monitoring the test specimens and other contributions to experiments.

For their generous contributions to our study, I would like to give thanks to MSc. Muhammed MARAŞLI and Fibrobeton Building Components Industry Const. Inc.

I would love to express my thanks to Prof. Dr. Alper İLKİ for valuable suggestions during design and test of the specimens.

I would like to offer special thanks to my father Bekir ÖZDEMİR, who always wanted me to follow the path of science and supported me in all circumstances, and my mother Bircan ÖZDEMİR, who always stood by me with all her means and never spared her efforts.

My special thanks to my lovely little sister Benay ÖZDEMİR, whose make me feel better in my worried times with her funny moments.

The most special thanks to my dear fiancé Gözde ÜNLÜ for her support, love and being always by my side.

ABSTRACT

LARGE SCALE TESTING OF MASONRY WALLS UNDER THE EFFECTS OF REPRESENTATIVE GROUND SETTLEMENTS

Several methods have been proposed so far with varying sophistications to predict ground settlement-related building damage. Limiting Tensile Strain Method (LTSM) is one of them and is frequently used in practical risk assessments. However, this method and several other methods developed based on a beam analogy might become insufficient (conservative or non-conservative) in building damage predictions due to their inherent simplicity. The accuracy of LTSM can be improved by revealing its limitations through experimental tests. However, a quite limited number of studies have been devoted so far to the investigation of soil-structure interaction caused by excavations. On the other hand, most of these studies have been performed by using small-scale building specimens.

In this thesis, four large-scale structural tests have been conducted on load-bearing masonry walls. Ground displacements have been represented as support movements. Owing to realistic scale (1/2) of the walls, the effect of material properties, wall constructions, connection details and loadings could be represented in a more realistic way. The effects of floor stiffness and wall openings were examined. A comprehensive monitoring scheme could also be carried out for displacements and strains using different techniques. Based on monitored data, damage measures have been determined. Analytical predictions made through the LTSM in regard to the damage class of the walls were compared to observed damage states.

Results demonstrate that the floor type has a considerable effect on the wall response and the extent of the settlement damage and damage propagation. As the number of the openings in masonry walls increases, a more distributed crack pattern is observed. Analytical predictions made through LTSM incorporated with different stiffness relations have e general agreement with actual wall damages. Nevertheless, due to use of fictitious beam approach, the accuracy of LTSM is highly affected by the structures' floor type.

ÖZET

YIĞMA DUVARLARIN ZEMİN OTURMASINI TEMSİL EDEN ETKİLER ALTINDA BÜYÜK ÖLÇEK TESTLERİ

Tünel kazıları zemin oturmalarına neden olabilir ve bu oturmalar yüzey yapılarına zarar verebilir. Tünel çalışmaları öncesinde, zemin oturmasından kaynaklanan riskleri analiz etmek için hesaplamalar kullanılarak gerekli hasar tahminleri yapılmalıdır. Zemin oturmalarına bağlı bina hasarını tahmin etmek için şimdiye kadar farklı seviyede detayları barındıran çeşitli yöntemler önerilmiştir. Sınır Çekme Şekildeğiştirmesi Metodu (LTSM) bunlardan biridir ve pratik risk değerlendirmelerinde sıklıkla kullanılır. Ancak, bu yöntem ve kiriş analojisine dayalı olarak geliştirilen diğer birkaç yöntem, yapısal basitlikleri nedeniyle bina hasar tahminlerinde yetersiz (aşırı muhafazakâr veya güvenli olmayan tahminler yaparak) kalabilir. LTSM'nin doğruluğu, deneysel testler yoluyla sınırlamaları kapsamlı olarak incelenerek geliştirilebilir. Ancak kazıların neden olduğu zemin-yapı etkileşiminin araştırılmasına yönelik az sayıda deneysel çalışma yapılmıştır. Öte yandan bu çalışmaların çoğu küçük ölçekli yapı örnekleri kullanılarak gerçekleştirilmiştir.

Bu tezde, taşıyıcı yığma duvarlar kullanılarak dört büyük ölçekli yapısal test gerçekleştirilmiştir. Zemin yer değiştirmeleri mesnet hareketleri olarak tatbik edilmiştir. Duvarların gerçekçi ölçeği (1/2) sayesinde malzeme özellikleri, duvar inşa teknikleri ve yükler daha gerçekçi bir şekilde temsil edilebilmiştir. Döşeme rijitliğinin ve duvar açıklıklarının etkileri incelenmiştir. Farklı teknikler kullanılarak yer değiştirmeler ve şekildeğiştirmeler için kapsamlı bir yapı sağlığı izleme prosedürü de uygulanmıştır.

Sonuçlar, döşeme tipinin duvar davranışı, oturma hasarının boyutu ve hasar dağılımı üzerinde önemli bir etkiye sahip olduğunu göstermektedir. Yığma duvarlarda boşluk arttıkça daha dağılı bir çatlak örüntüsü gözlenmiştir. Farklı rijitlik ifadeleri kullanılarak modifiye edilmiş LTSM aracılığıyla yapılan analitik tahminler, gerçek duvar hasarları ile genel olarak uyumludur. Bununla birlikte, basit kiriş yaklaşımının kullanılması nedeniyle, LTSM'nin doğruluğu, yapıların döşeme türünden büyük ölçüde etkilenmektedir.

TABLE OF CONTENTS

LIST OF FIGURES

Figure **Page**

Figure **Page**

LIST OF TABLES

Table **Page**

Table **Page**

CHAPTER 1

INTRODUCTION

1.1. Introduction and Scope of Study

In order to predict settlement-induced building damage, various analyses were performed using analytical, semi-numerical and numerical methods. Limiting Tensile Strain Method (LTSM) is one of the well-known analytical calculations which was developed by Burland and Wroth (1974). As an example, to semi-numerical methods, the Relative Stiffness Method (RSM) that was developed by Potts and Addenbrooke (1997) can be given. Their study suggests the incorporation of modification factors within the classical LTSM to consider soil-structure interaction. The modification factors were derived by means of extensive numerical analyses. The most detailed analyses can be done using numerical methods. While the coupled (both soil and building are involved in the numerical model and their interactions are taken into considerations in the analyses) (Amorosi et al., 2014) and semi-coupled (excavation-induced ground displacements are applied as prescribed displacements and interaction is taken into account through structural bedding interfaces) (Giardina et al., 2013) numerical analyses provide the most realistic results. The un-coupled (soil-structure interaction is neglected) numerical analyses have been used in early researches for the old masonry buildings that are incapable of modifying ground displacements.

In addition to modelling studies, there are also experimental studies in the literature. These studies were performed to investigate the effects of wall base or foundation movements on masonry and concrete frame specimens. Investigations of Laefer et al. (2011), Giardina et al. (2012) and Ritter et al. (2017) can be given as examples to experimental studies. Despite valuable contributions, these studies had serious limitations because of the model scales, material properties, specimen production techniques and the number of test specimens.

The current study aims at filling the lack of large-scale experimental study in this field. Compared to the previous studies, larger scale masonry wall specimens with the more realistic details like the presence of actual floor system are constructed and tested. Test results are utilized to evaluate the global structural response to applied artificial settlements, damage mechanisms and propagations, influences of the window openings and different floor types. In addition, one specimen is tested after being retrofitted to investigate the possibility of enhanced settlement performance of the relevant specimen. Experimental results (except for the retrofitted specimen) are also used to assess the predictions of the current LTSM in regard to the final damage class. To this end, structural stiffness is calculated using different approaches suggested by several researchers. The improvement of the analytical prediction methods through the validations to be made by comparing with the experimental results is significantly important for accurate building settlement damage classification. Enhanced accuracy will provide the following potential benefits. In this way, not only an effective damage prevention is provided, but also the project budget and time will be used more efficiently.

- Building damage is predicted more successfully: The number of cases concluded with over-or underestimated damage results is minimized. This means that the extent of the damage protection measures regarding the infrastructure activities like excavation supports can be reasonably and realistically optimized.

- The need for detailed analysis is decreased: When the accuracy of current analytical methods is increased, their reliability will increase. Therefore, the less number of the buildings will require rigorous modelling and analysis procedures.

1.2. Thesis Organization

This thesis is presented in six chapters: Introduction, Literature Review, Preparations prior to experiments, Experimental Study, Wall Settlement Tests, Results, and Conclusion.

Chapter 2 presents literature review which describes ground settlements caused by tunnelling, deformation measures, Limiting Tensile Strain Method, laboratory experiments to investigate the structural response to representative ground settlements.

Chapter 3 presents preparations made for the experimental study which includes design of settlement test setup, design of masonry walls used in tests, loading combinations and monitoring techniques.

Chapter 4 presents settlement tests on reference specimen, on joist floor specimen and on combined specimen.

Chapter 5 presents the performed analytical calculations by using Limiting Tensile Strain Method (LTSM) with various stiffness calculation approaches suggested previously.

Chapter 6 presents results of analytical calculations and comparisons with experimental results.

In Chapter 7 consists of conclusions derived from the current study and presents the recommended further studies.

CHAPTER 2

LITERATURE REVIEW

2.1. Ground Settlements Caused by Tunnelling

Tunneling and deep excavation activities usually result in ground movements in vertical and horizontal directions. Ground settlement can be defined as the vertical movements of the ground. These movements are caused from changes in stresses within the soil. Boscardin (1980) states that a change in stress state in the ground, ground loss, and any decrease or increase in the groundwater regime are the major reasons of ground movements induced by excavation. According to Son (2003), size of excavation, construction technique, type and stiffness of soil, face stability of the tunnel and properties of supporting system are important factors affecting the magnitude of excavation-induced ground movements. Since the ground movements may damage to structures, building damage predictions become important. Therefore, excavation-induced building damage predictions should be performed accurately.

According to Potts and Addenbrooke (1997), there is an interactive relation between structures and soil. Burd et al. (2000) stated that by utilizing their overall stiffness, structures can resist to ground movements occurred by excavation activities in their neighborhood. According to Comodromos et al. (2014), for the structures which have stiff foundations, the magnitude of horizontal and vertical ground movements may decrease, and because of restraint effect of the foundations, settlement profile may become a widened trough shape. In addition, Potts and Addenbrooke (1997) states that presence of stiff structure restraints the horizontal movement of soil. Moreover, according to Burland and Wroth (1974), the foundations of many buildings provide a significant restraint to deformations.

Ground movements are estimated for a place where the buildings are absent, these are called free-field or green-field settlements. In preliminary assessment stage, damage

predictions which are calculated considering free/green field ground movements can inform about the vulnerability of many buildings in the areas which are influenced by excavation. Peck (1969) suggested that the free/green field ground movements in the transverse direction caused by tunnelling activities can be represented by the Gaussian Normal Distribution Curve Method. This method is a common semi-empirical technique which is used for many years. Free/green field surface profiles perpendicular to the tunnel line are named as settlement troughs. Figure 2.1 shows the Gaussian Normal Distribution Curve Function, where $S_v(x)$ is the vertical ground movement, $S_{v,max}$ is the maximum vertical ground movement just above the tunnel axis, $S_h(x)$ is the horizontal ground movement, z_0 is the vertical distance between the ground surface and the center of the tunnel, i_x is the horizontal distance between the inflection point and the vertical axis. Equation (2.1) helps to calculate the vertical ground movement at a point in the settlement profile.

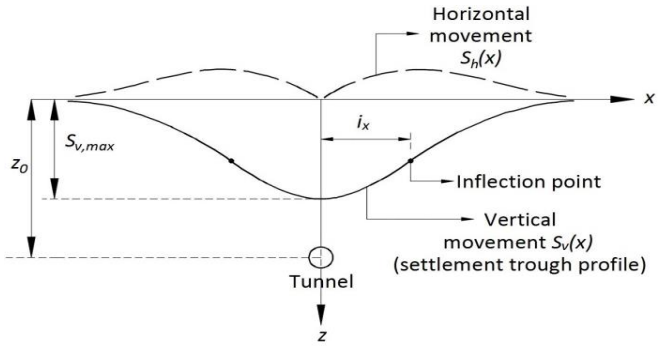

Figure 2.1. Gaussian Normal Distribution Curve Function (Source: Dalgic et al, 2017; (modified from Peck, 1969))

$$S_v(x) = S_{v,max} e^{-\frac{x^2}{2i_x^2}} \tag{2.1}$$

Settlement trough consists of concave or convex parts (Figure 2.1). Concave part of the profile is named as sagging, convex part of the profile is named as hogging. According to Comodromos et al. (2014) and Potts and Addenbrooke (1997), structures can be located at different positions with respect to tunnel line and they could modify ground settlements depending on their restraint abilities such as weight, size, and foundation type. Figure 2.2 shows the different buildings which are in sagging (i), in the

vicinity of the inflection point (ii) and in hogging (iii). In figure, *e* represents the eccentricity between the center of the building and the tunnel center (Dalgic et al, 2017).

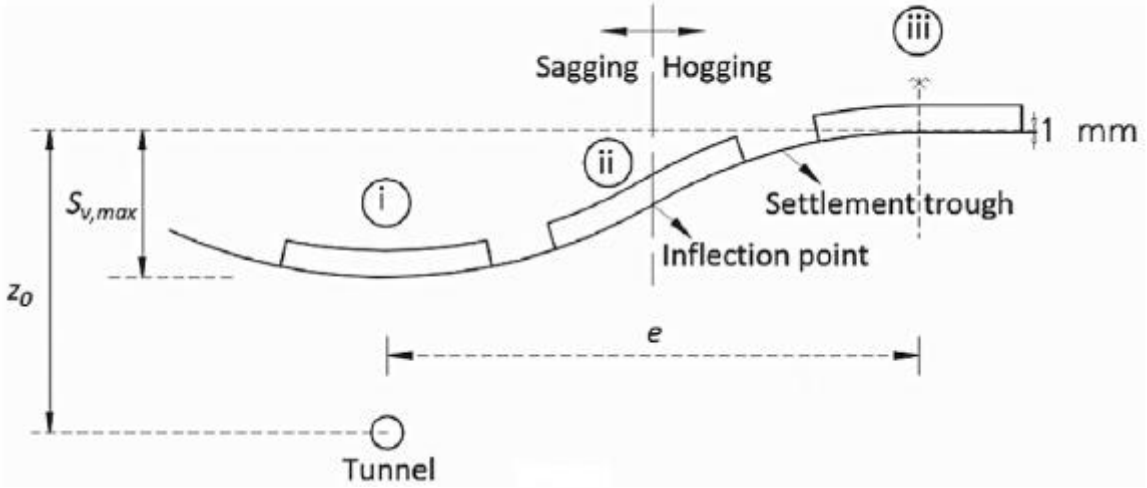

Figure 2.2. Different positions of buildings in the transverse settlement trough: (i) sagging, (ii) at an inflection point, (iii) hogging. (Source: Dalgic et al, 2017)

2.2. Deformation Measures

Several deformation measures were adopted in the literature so far. They show the measurable quantities that are used to evaluate the structural response to an excavation-induced ground movement. Estimated ground settlement contours obtained at the foundation level, or site measurements performed on the existing structures can be used for calculating building deformation measures. According to Peck et al. (1956) and Little (1969), structural damage of the buildings can occur when they are subjected to differential settlement. Herein, the differential settlement corresponds to a vertical ground movement that differs from one end to another of the relevant structure. The columns of framed structures and the walls of masonry structures can be subjected to differential settlements along their sides. In the literature, there are three common damage measures: differential settlement (δS_v), angular distortion (β) and deflection ratio (Δ/L). Figure 2.3 represents these three damage measures for a masonry wall conforming to ground settlement profiles in different zones (Dalgic et al, 2017).

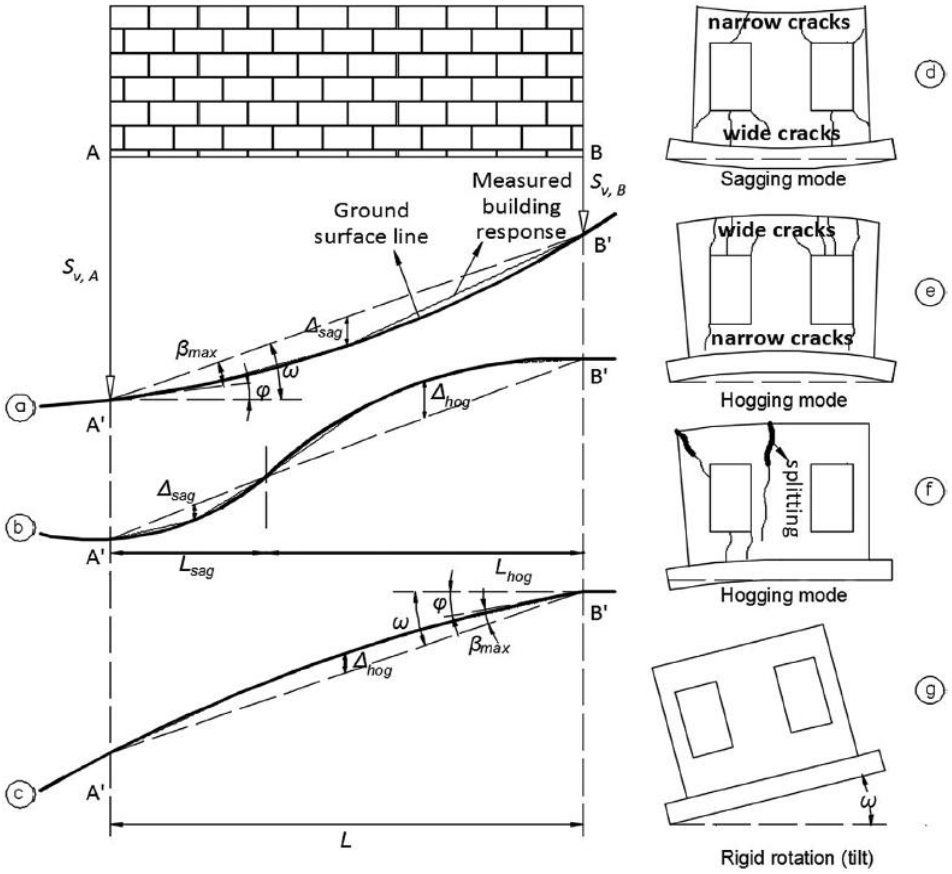

Figure 2.3. Deformation measures for a masonry wall conforming to a ground settlement profile in: (a) the sagging zone, (b) both the sagging and hogging zones, and (c) the hogging zone and the typical building damages or responses (d, e, f, and g). (Source: Dalgic et al, 2017)

In case of tunnelling activities causing the ground settlement, points A and B moves toward to points A' and B', and this motion may generate straining in the wall if building experience any distortion. Equation (2.2) can be used to calculate the differential settlement (δS_v) between the points A' and B'. Here, $S_{v,A}$ and $S_{v,B}$ are the absolute vertical displacements of points A and B, respectively.

$$\delta S_v = S_{v,A} - S_{v,B} \tag{2.2}$$

Other deformation measure is angular distortion (β). For the first time, it was suggested by Skempton and McDonald (1956) as a driving parameter related to excavation-induced building deformation. Here, β is equal to the differential settlement

(δS_v) divided by considered length of the structure (distance between the points A and B). Equation (2.3) demonstrates this relation:

$$\beta = \frac{\delta S_v}{L} \tag{2.3}$$

Afterwards, Boscardin (1980) suggested that the rigid rotation of building (ω) should be excluded in the calculations. To find modified β, the slope of the settlement profile (φ) becomes necessary. Equation (2.4) shows the modified angular distortion (β) relation according to the suggestion of Boscardin (1980). It should be noted that, in recent studies, shear strain calculated based on vertical and horizontal differential strains of represented structures may be used as a measure of angular distortion.

$$\beta = |\omega - \varphi| \tag{2.4}$$

The other deformation measure is the deflection ratio (Δ/L) which was proposed by Polshin and Tokar (1957). As demonstrated in Figure 2.3, Δ is the distance between displaced foundation line and the linear line connecting points *A'* and *B'*, and L is the considered length of the structure. Mair et al. (1996) suggested that, for structures located both in hogging and sagging parts of a settlement trough, Δ/L can be calculated separately for both parts (Figure 2.3)

Deformation measure to be accounted in the evaluations should be chosen in compliance with estimated deformation mode. Netzel (2009) suggested that for the cases in which bending related damage is more likely, the deflection ratio (Δ/L) is more suitable. Whereas, if anticipated damage is shear related, the angular distortion (β) can be used.

2.3. Limiting Tensile Strain Method (LTSM)

2.3.1. Building risk assessment procedure

Analytical methods like the Limiting Tensile Strain Method (LTSM) are based on structural engineering calculations and used to estimate the risk level of the buildings in case of ground movements induced by excavation. For this purpose, building response is firstly predicted considering either free field or modified ground movements and then

calculated response is assessed through threshold values pre-defined in terms of principal tensile strain and slope of the building.

According to Mair et al. (1996), the risk assessment process consists of three stages: preliminary assessment, second-stage assessment, and detailed evaluation. In the preliminary assessment stage, at first, settlement contours are obtained using numerical tools or site measurements. After that, buildings that to be probably subjected to vertical settlements less than 10 mm at any point of the structures are eliminated from the risk assessment. These eliminated buildings are also checked that the ground slope at their relative positions should not exceed 1/500. The buildings that pass the preliminary assessment are included in the second and detailed assessment stages. In the second assessment stage, analytical methods such as Limiting Tensile Strain Method (Burland and Wroth, 1974), Laminate Beam Method (Finno et al., 2005), or semi-numerical methods such as Relative Stiffness Method (Potts and Addenbrooke, 1997) are performed for those buildings. If the buildings are categorized in moderate or high-risk classes in the second stage, then they are re-evaluated in the detailed assessment stage. In the detailed assessment stage, more sophisticated methods like finite element numerical methods are performed. In most cases, the risk decision for most of the buildings considered is made in the second assessment stage and only few buildings which are in very unfavorable positions or having critical importance require detailed assessment. Therefore, the accuracy of the decisions made in the second assessment stage is highly important. Improving the capability and reliability of analytical methods used in the second assessment stage will not only provide an effective damage prevention, but also will benefit the efficient use of project budget and time.

2.3.2. LTSM

The Limiting Tensile Strain Method (LTSM) is an analytical method which is used in the second assessment stage for damage prediction of structures subjected to excavation-induced ground movements. Burland and Wroth (1974) developed the research of Polshin and Tokar (1957) and suggested a fictitious beam model for frame and masonry structures to compute tensile strain values. Structures are modeled as elastic beams in rectangular shape and without weight. In this approach, when the foundation of

structure is subjected to ground movements induced by tunnelling activities, it is assumed that the deformation demand is entirely transmitted to the upper structure without considering any reduction due to soil-structure interaction (Netzel, 2009). This assumption refers that the structure is subjected to differential settlements which can cause the large distortions and high strain values. Following the calculations of tensile strains, these values are compared to the limiting strain thresholds that address to the building damage classes.

The fictitious beam model considered by Burland and Wroth (1974) is shown in Figure 2.4. *L* is the length of the beam (refers to considered length of the real building) and *H* is the height of the beam (refers to height of the real building from the foundation to the top).

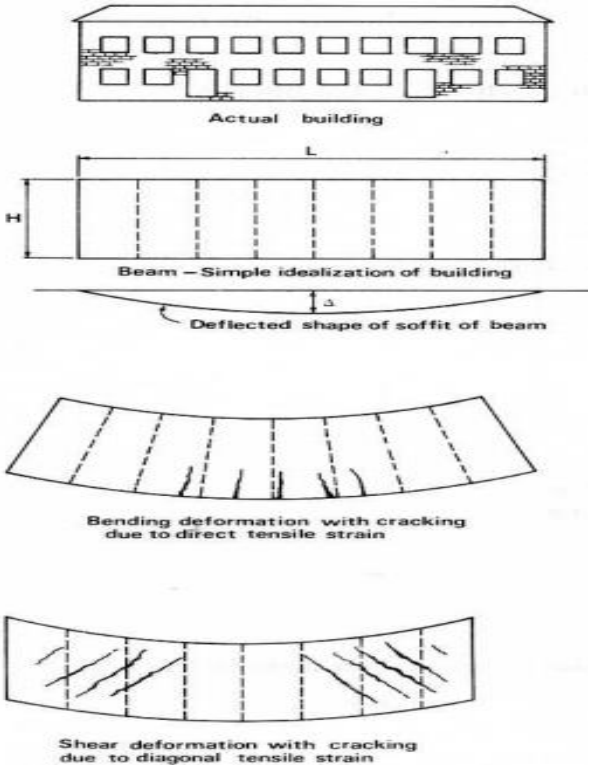

Figure 2.4. The model of the fictitious beam (Source: Burland and Wroth, 1974)

Timoshenko (1957) suggested Equation (2.5) for total central deflection of a centrally loaded beam of unit thickness flexing both shear and bending.

$$\Delta = \frac{PL^3}{48EI}\left[1 + \frac{18EI}{L^2HG}\right] \quad (2.5)$$

Herein, *E* is the elasticity modulus, *G* is the shear modulus, *I* is the second moment of the area of the beam and *P* is the given load. When the vertical settlement response of a structure is considered (Figure 2.4), *P* in Equation (2.5) does not refer to a real central load. Actually, *P* has to be thought as a factor which brings out a deformation mode in case of a ground settlement. Burland and Wroth (1974) examined two more alternative cases for loading type and deformation mode to verify the appropriateness of the mentioned central loading for the use of this equation in the simulation of ground settlement problem: uniformly distributed loading and a circular beam deflection mode. It was observed that the initial cracking of the beam model was not influenced by the alternative applications of loading type and deflection mode. Then, they suggested using Timoshenko's (1957) beam equation as is with the consideration of fictitious central loading *P* because of its simplicity.

Equations (2.6) and (2.7) were developed by Burland et al. (1977) by rewriting the Equation (2.5) to reveal the relationship between Δ/L and the maximum tensile strains (ε_{bmax} and ε_{dmax}) which indicate the cracking potential of the building walls in either bending or diagonal tension. Equation (2.5) can be formed in terms of maximum longitudinal (used for bending critical cases) and diagonal (used for shear critical cases) tensile strains as seen in Equations (2.6) and (2.7), respectively. When Δ/L and ε_{bmax} are isolated, Equation (2.5) can be rewritten as:

$$\frac{\Delta}{L} = \left[\frac{L}{12t} + \frac{3EI}{2tLHG}\right]\varepsilon_{bmax} \tag{2.6}$$

Here, ε_{bmax} is the maximum extreme fiber strain. Equation (2.6) can be used for building cases in sagging or hogging. *t* shows the neutral axis depth of the fictitious beam model.

Similarly, Equation (2.5) can be re-expressed in terms of maximum diagonal tensile strain:

$$\frac{\Delta}{L} = \left[1 + \frac{HL^2G}{18EI}\right]\varepsilon_{dmax} \tag{2.7}$$

Here, ε_{dmax} is the maximum diagonal tensile strain.

Burland and Wroth (1974) assumed that the neutral axis could be considered at the center of the fictitious beam model for sagging structures. By this consideration, the depth of neutral axis (t) is equal to H/2. Site observations supported this assumption i.e. settlement-induced vertical cracks are more severe in general up to the mid-height of the

walls. However, because of absence of strong foundation system in historical masonry structures, vertical cracks can be observed at the parts of the building close to the foundation due to sagging. They adopted $\mathrm{E/G} = 2 \times (1 + \nu)$ for an isotropic elastic material and took the Poisson's ratio (ν) as 0.3. Thus, the *E/G* ratio becomes 2.6. According to the suggestion of Timoshenko (1957), the second moment of inertia was taken as $\mathrm{I} = 1 \times H^3/12$ by considering a unit width. Equation (2.8) and (2.9) show the relationships between Δ/L and the maximum tensile strains in sagging.

$$\frac{\Delta}{L} = \left[0.167\frac{L}{H} + 0.65\frac{H}{L}\right]\varepsilon_{bmax} \qquad \text{(for bending in sagging)} \qquad (2.8)$$

$$\frac{\Delta}{L} = \left[1 + 0.25\frac{L^2}{H^2}\right]\varepsilon_{dmax} \qquad \text{(for shear in sagging)} \qquad (2.9)$$

Burland and Wroth (1974) assumed a neutral axis position at the bottom edge of the fictitious beam model ($t=H$) for the structures in hogging. According to them, this assumption may be more realistic due to significant restraint effect of building foundations to deformations. In other words, the parts of the wall above the foundation line are assumed to be subjected to tensile effects. Son and Cording's (2007) finite element analysis results supported this assumption later on. For hogging cases, the relationships between Δ/L and the maximum tensile strains were established by Burland and Wroth (1974) as shown in Equations (2.10) and (2.11). The second moment of inertia (I) is re-calculated based on the new location of neutral axis, and it is found as $H^3/3$. The relative stiffness (E/G) can be taken same as in the case of sagging, 2.6.

$$\frac{\Delta}{\mathrm{L}} = \left[0.083\frac{\mathrm{L}}{\mathrm{H}} + 1.3\frac{\mathrm{H}}{\mathrm{L}}\right]\varepsilon_{\mathrm{bmax}} \qquad \text{(for bending in hogging)} \qquad (2.10)$$

$$\frac{\Delta}{\mathrm{L}} = \left[0.064\frac{\mathrm{L}^2}{\mathrm{H}^2} + 1\right]\varepsilon_{\mathrm{dmax}} \qquad \text{(for shear in hogging)} \qquad (2.11)$$

According to Burland and Wroth (1974), maximum tensile strain [max ($\varepsilon_{bmax}, \varepsilon_{dmax}$)] is the more convenient quantity to determine the initiation of visible cracking in load-bearing masonry walls and infilled walls of frame structures. Experimental studies (Burhouse, 1969; Mainstone and Weeks, 1970; Mainstone, 1974) showed that the tensile strain at the onset of cracking in any direction can be considered as 0.05%-0.1% for both masonry and brick infill walls.

Burland et al. (1977) suggested a damage classification table, then Boscardin and Cording (1989) modified it (Table 2.1). Here, column of damage category refers to

Skempton and Macdonald's classification (1956). They divided the building damages into three categories: architectural damage, functional damage, and structural damage. The other columns are constructed by Burland et al. (1977) and Boscardin and Cording (1989). The values listed in this table are suggested based on the observed approximate width of cracks.

Table 2.1. Damage Classification Table (Source: modified from combining Skempton and MacDonald's (1956) damage category and the study of Boscardin and Cording (1989))

Damage Category	**Class of Damage**	**Description of Damage**	**Approximate width of cracks, mm**
Architectural	Negligible	Hairline cracks	< 0.1 mm
	Very Slight	Fine cracks	< 1 mm
	Slight	Cracks easily filled	< 5 mm
Functional	Moderate	The cracks may require cutting out and patching	5 to 15 mm, or several cracks > 3 mm
	Severe	Extensive repair work is required. Utility service disrupted	15 to 25 mm also depends on number of cracks
Structural	Very Severe	Major repair required. Beams lose bearing walls lean badly and require shoring.	Usually > 25 mm depends on number of cracks

After Boscardin and Cording (1989), this table was modified by involving the added limiting tensile strain intervals ($\varepsilon_{lim(low)}$, $\varepsilon_{lim(up)}$). The result of Equation (2.6) or (2.7), for the values of ε_{bmax} and ε_{dmax}, whichever is greater, is taken and compared with the limiting values listed in Table 2.2 to determine the corresponding final damage class.

Table 2.2. Damage Classification Table (Source: Dalgic et al (2017) modified from Burland et al. (1977) and Boscardin and Cording (1989))

Category of damage	**Damage class**	**Description of typical damage and ease of repair**	**Approximate crack width (mm)**	**ε_{lim} (%)**	
				After Boscardin and Cording (1989)	
				$\varepsilon_{lim\ (low)}$	**$\varepsilon_{lim\ (up)}$**
Aesthetic damage	0-negligible	Hairline cracks	Up to 0.1 mm	0.000	0.050
	I-very slight	Fine cracks that can easily be treated during normal decoration	Up to 1 mm	0.050	0.075
	II-slight	Cracks can be easily filled. Cracks are visible externally	Up to 5 mm	0.075	0.150
Functional damage affecting serviceability	III-moderate	The cracks require some opening up and can be patched by a mason	5-15 mm or a number of cracks larger than 3 mm	0.150	0.300
	IV-severe	Includes large cracks. Extensive repair work is required	15-25 mm but also depends on the number of cracks	>0.300	
Structural damage affecting stability	V-very severe	Beams lose bearing, walls lean and require shoring, and there is a danger of structural instability	Usually larger than 25 mm but also depends on the number of cracks	>0.300	

2.3.3. Effects of horizontal strains on LTSM

Incorporation of horizontal strains into LTSM calculations decreases Δ/L value that a building can tolerate without cracking (Boscardin and Cording, 1989). It means, when the horizontal strains are added into calculations, initiation of damage occurs at smaller values of Δ/L, thus, higher damage classes can be observed for a given Δ/L. However, in this paper, effect of horizontal strains is not considered since their effect was found insignificant in the current masonry wall tests. The reason for having low level of

horizontal strains affecting the walls might be attributed to the low level of shear stress transfer realized between settlement test setup and wall specimens.

According to Son and Cording (2005), the combined tensile strain (ε_t) is calculated as shown in Equations (2.12) and (2.13). They combined the average horizontal strain (ε_h) with the values of maximum bending strain (ε_{bmax}) and the maximum shear strain (ε_{dmax}). In Equation (2.12), average horizontal strain can be summed directly with the maximum longitudinal tensile strain.

$$\varepsilon_t = \varepsilon_{bmax} + \varepsilon_h \tag{2.12}$$

However, for shear critical case, average horizontal strain cannot be summed with the maximum shear strain, directly. They are combined using Mohr's Circle as shown in Equation (2.13).

$$\varepsilon_t = \frac{\varepsilon_h}{2} + \sqrt{\left(\frac{\varepsilon_h}{2}\right)^2 + \varepsilon_{dmax}^2} \tag{2.13}$$

It should be noted that, the combined tensile strain (ε_t) values in Equation (2.12) and (2.13), whichever is greater, is compared with the limiting values in Table 2.2, then damage class is observed after this comparing.

To include these findings into the LTSM equations, according to suggestions of Boscardin and Cording (1989), Equations (2.14) and (2.15) is used. For bending critical case in a hogging zone, the relationship between Δ/L and the maximum bending strain with horizontal contribution is shown in Equation (2.14). It is found by substituting Equation (2.12) into Equation (2.10).

$$\frac{\Delta}{L} = \left[0.083\frac{L}{H} + 1.3\frac{H}{L}\right][\varepsilon_{bmax} + \varepsilon_h] \tag{2.14}$$

For shear critical case in a hogging zone, the relationship between Δ/L and the maximum shear strain with horizontal contribution is shown in Equation (2.15). It is found by substituting Equation (2.13) into Equation (2.11).

$$\frac{\Delta}{L} = \left[0.064\frac{L^2}{H^2} + 1\right]\left[\frac{\varepsilon_h}{2} + \sqrt{\left(\frac{\varepsilon_h}{2}\right)^2 + \varepsilon_{dmax}^2}\right] \tag{2.15}$$

2.3.4. Deficient sides of LTSM

LTSM is one of the most widely used analytical methods estimating excavation-induced building damages. However, due to its simplicity with regard to adopted beam approach and damage decision technique, it also has some deficiencies that need to be improved.

- Limitations regarding fictitious beam approach: The accuracy of the considerations of simply supported fictitious beam and central loading is limited by the length of the structure. When the length of the structure is too long or too short, this beam approach becomes insufficient (Finno et al., 2005)
- Negligence of effects of openings.
- Floor type is not taken into account.
- Self-weight of the structure is neglected.
- The soil-structure interaction is ignored: Actually, there is a dual interaction between soil and structures. Because of this neglection, the structural response is usually predicted in a more conservative way.

The results obtained by the researchers and site applications show that current analytical methods i.e., LTSM needs to be improved. This can be achieved by performing experimental tests in realistic scale and using building materials and architectural configurations as realistic as possible. The experimental tests will provide detailed data sets concerning the structure and its interaction with underlying media.

2.4. Laboratory Experiments to Investigate the Structural Response to Representative Ground Settlements

In recent years, limited number of experiments were conducted to examine the structural damages caused by excavations. Laefer et al. (2011) performed a pseudo-static, soil structure test by using $1/10^{th}$ scaled masonry walls. Figure 2.5 shows the wall used in the study of Laefer et al. (2011).

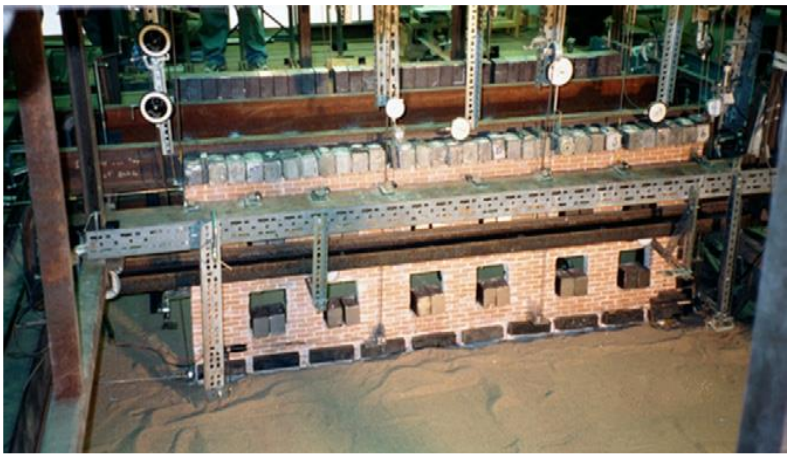

Figure 2.5. Test wall used in the study of Laefer et al. (2011)

To investigate the effects of excavations on masonry walls, they used a test bed filled with sand. Then, they simulated ground settlements caused by an adjacent excavation and focused on the response of the wall specimen. They reported that both ground movements and building damage patterns were in line with the targeted site measurements and findings of previous researchers.

Giardina et al. (2012) reported that laboratory tests provide a better understanding for the response of the structures subjected to support settlements and help to check the validity of computational models. The main aim of their experimental work was to provide accurate data that will be utilized for checking the validation of numerical analyses. They constructed a 1/10 scaled masonry wall specimen and then subjected to an artificial hogging-type settlement profile. The hogging-type settlement imitated the settlement effects caused by a tunnelling activity in the vicinity of the represented masonry building. The wall specimen was a representative of a typical Dutch house. The masonry wall specimen length, width and height are 1.5 m, 0.05 m and 1.2 m, respectively. As shown in Figure 2.6, the wall specimen was built on a steel I beam. I beam was connected to a fixed and rigid steel frame. Mentioned settlement profile was created by applying vertical displacements at one end of steel I beam.

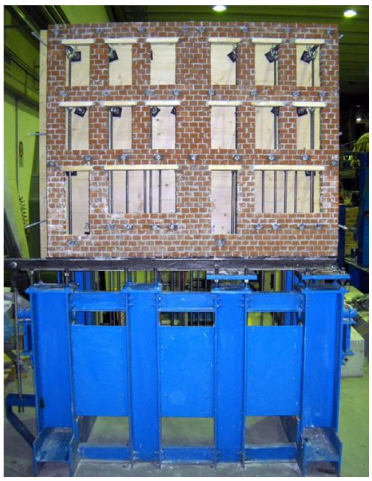

Figure 2.6. The wall specimen built on a steel beam (Source: Giardina et al., 2012).

After the experimental work done, the researchers performed analytical calculations by using LTSM to compare with the final damage results of the experimental test. However, the LTSM results underestimated the final damage. They stated that the reason of this was the very low mortar strength and presence of window openings which are not directly considered in the LTSM. Also, they remarked the importance of soil-structure interaction on the response of the structure.

Rittter et al. (2017) performed a series of centrifuge tests to research the settlement response of the masonry specimens. Specimens represented the surface structures subjected to ground settlement induced by tunneling activities in sand. Specimens were constructed by 3D printing adopting an adjusted material density to account for scaled stress states of small, printed walls. Figure 2.7 shows the one of the centrifuge specimens used in the experiments of Ritter et al. (2017).

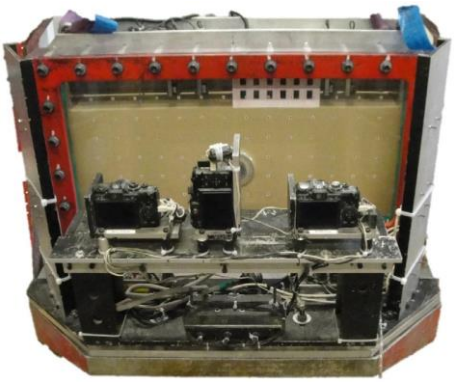

Figure 2.7. Front view of the centrifuge specimen (Source: Ritter et al., 2017).

Researchers also performed Relative Stiffness Method (RSM) and considered the stiffness reduction caused by window openings. Their experimental results showed that an increase in the ratio of façade openings reduces the bending stiffness, significantly. Also, the data showed that differential horizontal soil displacements around the test specimen reduced due to the presence of the wall structure, in general. They concluded that results of the simulation were in a good agreement with modelling in the perspective of volume changes in the soil, building position and façade openings.

CHAPTER 3

PREPERATION OF THE EXPERIMENTAL STUDY

The ground settlements that are induced by tunnelling activities poses a big risk on masonry structures. To understand the behavior of masonry structures, limited number of experiments have been conducted so far (Laefer et al., 2011; Giardina et al., 2012; Ritter et al., 2017). Although the effects of presence of openings, soil-structure interaction, scaling, and soil condition was investigated in these projects, it is obvious that there is still a need for experimental studies with a larger scale that will facilitate the further understanding of settlement response of the existing structures. In this way, the effect of essential characteristics of actual structures (material properties, architectural geometry, weight and connections) can be taken into account in a more realistic way. On the other hand, the global response of the walls and the development of damage patterns can be monitored in detail and gathered displacement and deformation data can be used to verify the existing damage assessment methods and to develop successful numerical models.

In this study, a series of large scale (1/2) masonry wall buildings (specimens) were constructed and tested. The specimens were the representative of the walls of Akaretler Row Houses (the prototype buildings) which were examined previously by Ispir and Ilki (2013). Akaretler Row Houses were built by the supports of Ottoman Court around 1875 in the south part of Istanbul nearby Bosphorus. According to the researchers, the Row Houses were one of the best examples of the civil architecture of their period because of neoclassical facades, ornaments, and location. Although the original load-bearing masonry walls were partly conserved, some parts of the existing floors were demolished. It is also reported that some vaulted floors were replaced with reinforced concrete (RC) slabs during the previous restorations (Ilki et al. 2007). Walls of row houses were made by solid clay bricks with varying dimensions of (19-26) × (10-13) × (4.5-7) cm^3. Bond pattern of masonry was cross-bond (English bond), and mortar joints were 10-35 mm thick in horizontal and 10-20 mm thick in vertical. The primary construction elements

were stone for foundations. A general view of Akaretler Row Houses, its load-bearing walls and RC slabs are presented in Figure 3.1.

(a) (b)

Figure 3.1. (a) General view of Akaretler Row Houses, (b) Load-bearing masonry walls and RC slabs of Akaretler Row Houses (Source: Ispir, 2010).

Akaretler Row Houses are a good example of masonry buildings that might be particularly vulnerable to excavation-induced ground settlements because of its long and continuous walls and relatively large window openings. On the other hand, it is a well-documented historical building by means of the previous studies (Ispir and Ilki, 2013). From these aspects, selecting this structure as the prototype of the test walls examined in the current study seemed a good option.

3.1. Design of Settlement Test Setup

In this experimental study, special test setups were designed, and the walls were subjected to incremental artificial differential settlements using these setups. Each wall building model (specimen) was composed of two parallel brick masonry walls, and reinforced concrete (RC) slabs that were connected these walls at two story levels. Figure 3.2 shows front and side views of a specimen used in this study as an example.

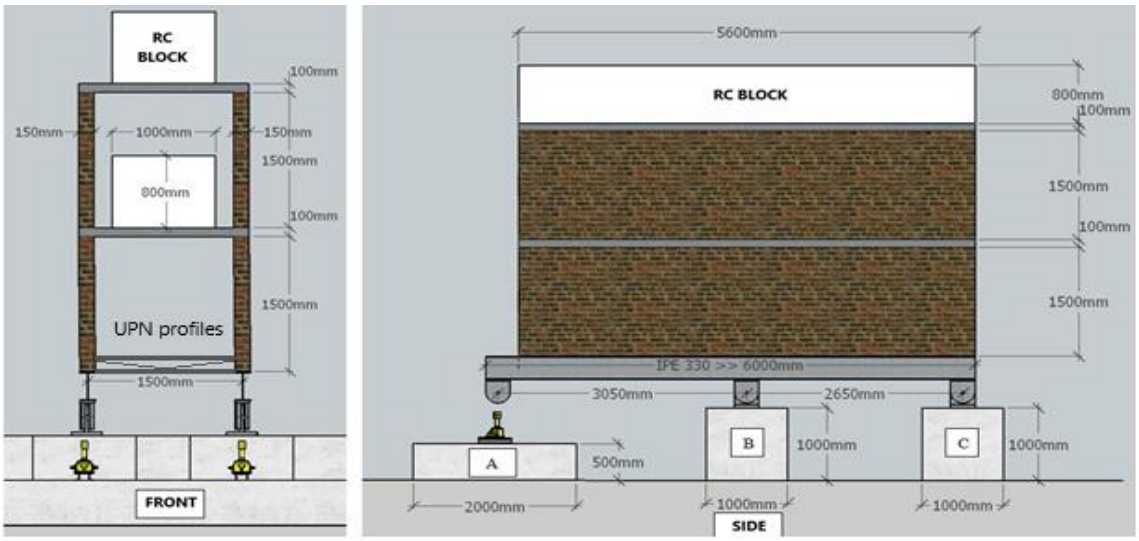

Figure 3.2. Front and side views of a specimen used in this study.

The specimens were constructed on two parallel steel beams (IPE330). Parallel beams were connected to each other by lateral cross-bracings (UPN profiles) to restrain out of plane movements and torsion. As shown in Figure 3.2, parallel beams were supported by three massive reinforced concrete blocks (A, B and C). Connections between parallel beams and reinforced concrete blocks were designed as moment-free pin connections considering estimated reaction forces. Base plates of pin connections were anchored to the reinforced concrete blocks via chemical anchors. Anchor details are shown in Figure 3.3.

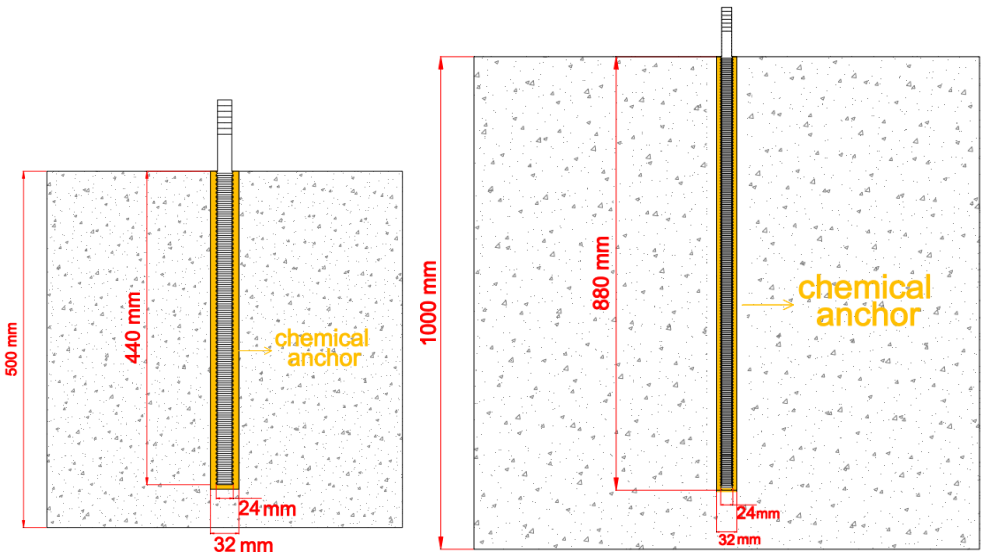

(a) (b)

Figure 3.3. Anchorage information of (a) support A, (b) supports B and C.

Since hogging type of ground settlements were more critical for masonry structures, a suitable scenario for tunnel construction and position of the building in the settlement trough was determined. To generate an experimental artificial hogging type of ground settlement, a tip displacement to the free ends of the steel beams were applied in downward direction. These tip displacements were applied through synchronous downward pulling forces by means of screw jacks located at support points A (shown in Figure 3.2) of the parallel steel beams. Figure 3.4 shows pin supports and movement principle of screw jacks.

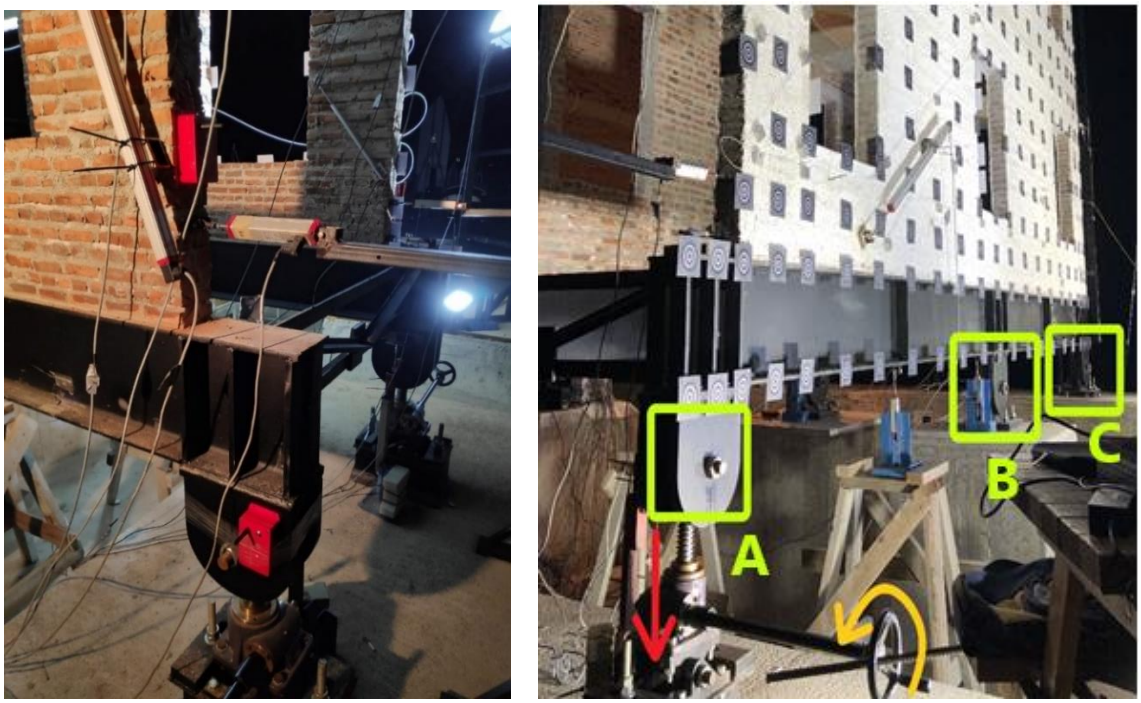

Figure 3.4. Pin supports and movement of screw jacks.

The damage potential can be measured as a ratio between the maximum vertical relative displacement and the effected length of the building (Δ/L). In the experiments, the ultimate Δ/L values experienced by IPE steel beams and walls changed between 2.5×10^{-3} (for walls) and 6.1×10^{-3} (steel beams). However, in the preliminary numerical analyses that had been performed to facilitate the design of the test walls and the experimental setup, the maximum deflection ratio (Δ/L) considered had been as around 5×10^{-3}. That value represented to a poor tunnelling scenerio. The Gauss Distribution Curve Parameters chosen to form such a tunneling case are shown in Table 3.1.

Table 3.1. Gauss Distribution Curve Parameters used to generate an artificial settlement profile.

Parameter	Description	Value	Unit
Sv,max	Max. Settlement	0.37	m
Vl	Volume Loss	0.05	-
D	Tunnel Diameter	12.2	m
i_x	Distance between inflection point and the tunnel center	6.25	m
K	Soil Parameter	0.25	-
Z_0	Tunnel depth	25	m

The variation of derived artificial vertical ground displacements in the hogging zone are shown in Figure 3.5. Herein, the magnitude of the maximum settlement is 122 mm. Considered horizontal distance is 11.2 m. The grey curve shown in this figure demonstrates the settlement profile that was applicable using the test setup. Note that the grey curve was determined as similar as possible to considered scenario curve indicated by the Gauss curve. Again, note that the magnitude of the settlements and the horizontal range in this figure is for actual scale 1:1. Due to scaling of the walls (1/2), applied values of both the magnitude of the settlements and the horizontal range should be considered as halves of these values.

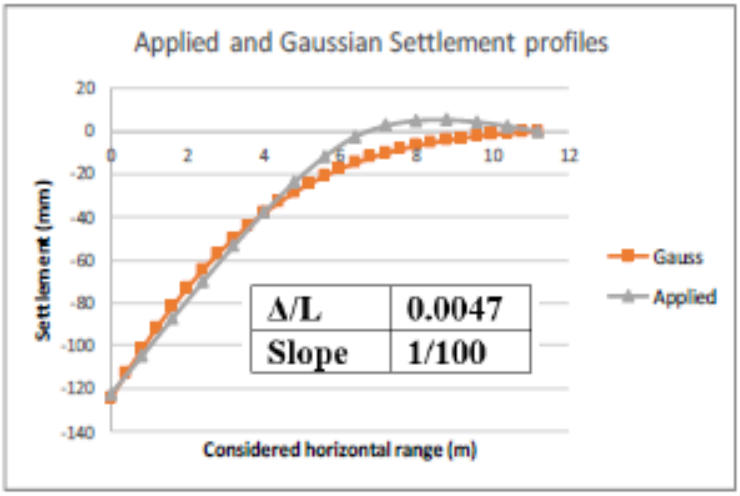

Figure 3.5. Applied and scenario settlement (Gauss) profiles (in Actual scale, 1:1).

3.2. Design of Masonry Walls

Four building specimens consisting of two parallel masonry walls were constructed to represent historical masonry structures built in the 19th century in Istanbul. For the construction of the walls, ½ scaling factor was adopted. Therefore, all the structural items including bricks and mortar joints were scaled accordingly. Scaled bricks were produced by cutting larger bricks. The final dimensions of cut bricks are 115x57.5x30 mm. Each wall had a height of approximately 3.2 m (includes two storeys) and the length of 5.6 m. The thickness of each wall was 0.115 m which corresponds to the length of one scaled brick.

In the design of the wall building models, window opening ratio (OR) of the walls and floor stiffness were the main test variables. In order to examine the effect of OR, masonry walls with OR of 35%, 20% and 0% were tested. The general view of specimens is shown in Figure 3.6.

Figure 3.6. The general view of specimens.

The reference building was identified as the specimen with three window openings (20% OR) and stiff RC floors. Second specimen consisted of 20% OR. In contrary to others, it had flexible floors. Third specimen was allocated for the investigation of a retrofitting application. It had the same geometry with the reference

wall however its walls were retrofitted before testing. The details and test results regarding the retrofitted specimen are not in the scope of this thesis. Fourth specimen consisted of a combination of the masonry walls with 0% and 35% OR's. It also had stiff RC floors. Table 3.2 shows the configurations of each wall building specimen.

Table 3.2. The configurations of each wall building specimen.

Specimen Name	**Features of Walls**	**Opening Ratio (OR)**	**Floor Type**
Reference	2 parallel similar walls	20 %	Stiff RC Floor
Retrofitted (Not in the scope)	2 parallel similar walls plus retrofitting	20 %	Stiff RC Floor
Joist Floor	2 parallel similar walls	20 %	Flexible RC Floor
Combined	2 parallel walls and different ORs for each wall	0% and 35 %	Stiff RC Floor

3.3. Additional Weights Considered in Tests

Previous research showed that building weight is a significant factor affecting the settlement response. As the building weight increases the buildings more likely tend to conform to the ground settlements. In other words, depending on the foundation type, masonry structures are more vulnerable to excavation-induced damages if they are heavier.

In this study, Artificial Mass Simulation theory of Krawinkler (1981) was considered in terms of scaling. Thus, to be able to represent the actual stress due to weight of the real prototype structure in the scaled specimen tests, an equal compressive stress state should be created at the bottom of the test walls. Therefore, specimens were loaded with heavy RC blocks through their floors. For the reference case, the compressive stress at the bottom of the walls was determined approximately 0.2 MPa.

The effect of building weight was simulated by increasing the amount of additional weight. While the effect of three different levels of building weight was investigated for the reference specimen, only two levels of building weight were considered for other specimens. The amount of additional weights and application details are presented in the following sub-sections.

3.3.1. Reference weight: RC Block Loading (W1)

Reference weight application (W1) was made by placing RC blocks on the floors of the specimens at two storey levels. In this way, both floors were loaded up to 7.8 tons (15.6 tons in total). Recall that W1 application corresponds to 0.2 MPa compressive stress level at the bottom of the parallel masonry walls. Reference, joist floor, retrofitted and combined building wall specimens were subjected to W1 in the first run of their settlement tests. Figures 3.7 (a), (b), (c) and (d) show RC block weights on reference, joist floor, retrofitted and combined wall specimens, respectively. It should be noted that first floor RC blocks had been placed during the construction of the walls and top floor RC blocks were placed before the settlement tests began. The RC block loading was executed very slowly and paying attention to symmetrical order of the loads to ensure a stress distribution as even as possible.

(a) (b)

(c) (d)

Figure 3.7. RC block loadings (a) on reference specimen, (b) on joisted specimen, (c) on retrofitted specimen (d) on combined specimen.

3.3.2. Nearly Doubled Weight (W2)

Increase of the building weight was simulated by increasing the amount of additional weight placed on the floors. To this end, in addition to RC blocks, extra weight was placed using sandbags and water tanks. Figure 3.8 shows nearly doubled weight reference specimen. It should be noted that, W2 was applied only for the reference building during its second run of settlement test. For W2, while the top floor was loaded up to 15.6 tons, the first floor was loaded up to 11.3 tons. Total added weight became 26.9 tons in total. W2 loading was achieved slowly and in a symmetrical order.

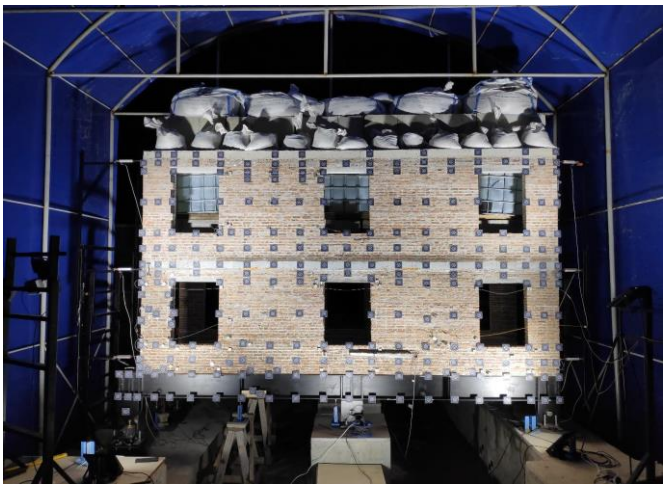

Figure 3.8. Nearly doubled weight (W2).

3.3.3. Extra Loading from Ground Floor Windowsills (W3)

As an extreme case, for only reference and retrofitted specimens an increased weight application was also made. In this case, extra weight was placed on the floors and windowsills of the ground floor of the specimens. Such a loading not only increases the total weight of the building but also escalates the damage vulnerability of the specimen because of changing stress states. For W3, total added weights on top floor, first floor and windowsills are 7.8, 7.8 and 3.3 tons, respectively. While top and first floors were loaded by RC blocks, water tanks were used to generate required weight that would be loaded through ground floor windowsills. For this purpose, steel profiles with hollow square box cross-section were placed transversely between the opposite windows and empty water tanks were put on these profiles. Afterwards, the tanks were filled with tap water. Figure 3.9 (a) and (b) show the application of W3 on the specimens of reference and retrofitted,

respectively. Also, Figure 3.9 (b) shows the detailed demonstration of application of W3. W3 loading was achieved slowly and in a symmetrical order.

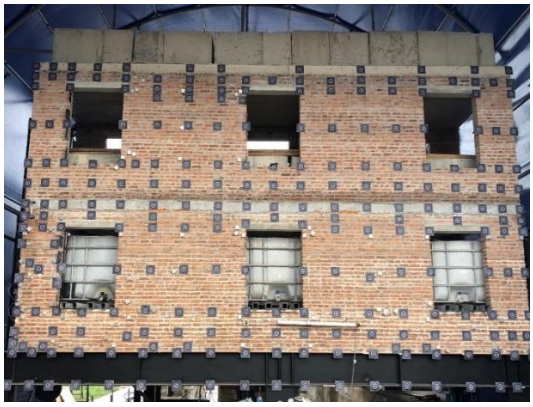

(a)

(b)

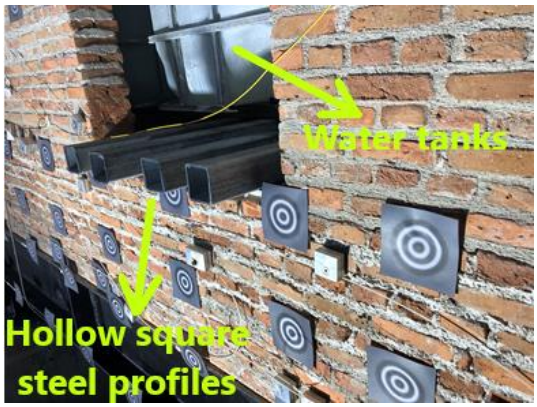

(c)

Figure 3.9. Application of W3: (a) on the reference specimen, (b) on the retrofitted specimen, (c) application of loads from the ground floor windowsills.

3.4. Monitoring Techniques Used in the Study

To monitor the settlement response of the specimens, different measurement techniques were used. Displacements, strains, crack widths, gapping width between IPE steel supports and the walls were measured. The data obtained through these techniques were compared and validated. Given that experimental studies are very rare in this field, acquired data will particularly be important to reveal and quantify the settlement response of masonry walls. In this thesis, measurements obtained only by Linear Variable Displacement Transducers (LVDTs) and Dynamic Monitoring System (DMS) are used. Crack openings were measured using crack rulers at several instants during the tests.

3.4.1. Instrumental Design of Monitoring Systems

LVDT

LVDTs were used to measure the displacements at different locations. Twelve LVDTs (6+6) were connected on the narrow sides (along the thickness of the walls) of the parallel walls at three different elevations (nearly bottom, mid-height and the top). As the walls move along with applied settlements, these LVDTs measured in-plane relative displacements of these points on the walls with respect to steel measurement towers standing next to the test setup and fixed to the ground independently. In-plane measurement will be used for the calculation of tilt of the specimens. While six LVDTs (3+3) in total facilitated to measure the vertical settlements on IPE steel beams, two of them were used to track the jack displacements at every step of incremental settlement loading. In addition, some extra LVDTs were also placed on the surface of the walls to measure the local crack openings and closures. One LVDT was always used to follow the out-of-plane displacements during the settlement tests. All the LVDTs were connected to TDG TEST BOX 1001 data logger. Data acquisition frequency was 1 sec. Figures 3.10 show the LVDT's installation plan to measure: (a) in-plane horizontal displacements, (b) in-plane vertical settlement displacements, (c) & (d) local crack openings and sliding.

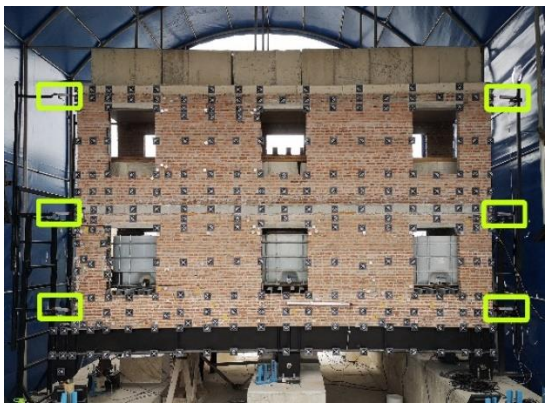

(a)

(b)

(c) (d)

Figure 3.10. LVDT's installed to measure: (a) horizontal displacements, (b) vertical displacements, (c) & (d) local crack openings and sliding.

DMS System

As a second displacement measurement technique, Imetrum's Dynamic Monitoring System (DMS) was used. This system was supplied and used by the partner team from the University of Oxford. It has capability of tracking the movement of each target point on the specimen in the test process. Additionally, this system supports the derivation of full-field strain maps by using the digital image correlation method (DIC). To perform the measurement accurately, there are five steps that should be applied:

- Choosing suitable location to set up the DMS system.
- Calculation of the required Field of View (FOV).
- Choosing of suitable camera and lens by considering the needed number of the cameras.
- Determination the target patterns.
- Determination the needed number of identical spotlights to obtain a uniform lighting on the specimen (D.B.Gulen, S.Acikgoz and H.Burd, 2019).

Note that only one of the parallel walls of each building specimen could be monitored by DMS. The wall monitored by DMS is called "front wall" throughout this thesis. Three of 4 cameras were placed in front of the front walls. These cameras were used for tracking the in-plane actions such as vertical and horizontal displacements and crack movements. Other camera was used to monitor out-of-plane displacements of the walls during the settlement tests. That one was placed in parallel to the pertinent wall and

tracked the target points located in the vertical windowsills. The placement of the cameras is shown in Figure 3.11.

Figure 3.11. Placement of cameras to observe reference building front wall.

CHAPTER 4

WALL SETTLEMENT TESTS

Settlement tests were executed at Fibrobeton Facility in Düzce/Turkey between the months of December and February in 2020-2021.

In total, seven settlement tests were performed for four building wall specimens. Five of them were examined in this thesis. Table 4.1 lists the test names and their features such as loading type. In this table, Tests 1, 2 and 3 show the reference specimen settlement tests carried out with W1, W2 and W3 weights, respectively. While Test 4 indicates settlement test of Joist floor specimen with W1 weight, Test 5 points out settlement test of Combined specimen with W1 weight. Given tip displacement was measured by both LVDT's and DMS system. The deflection ratio (Δ/L) values are calculated based on the DMS measurements.

Table 4.1. Test numbers and their properties.

TEST NUMBER	SPECIMEN NAME	GRAVITY LOADING TYPE	LOADING DEFINITION
Test 1	Reference	W1	*7.8 tons on top floor, *7.8 tons on second floor.
Test 2	Reference	W2	*15.6 tons on top floor, *11.25 tons on second floor.
Test 3	Reference	W3	*7.8 tons on top floor, *7.8 tons on second floor, *3.25 tons on windowsills of first floor.
Test 4	Joist Floor	W1	*7.8 tons on top floor, *7.8 tons on second floor.
Test 5	Combined	W1	*7.8 tons on top floor, *7.8 tons on second floor.

4.1. Reference Specimen Tests (Test 1, Test 2 and Test3)

Reference specimen consisted of two identical parallel walls. This specimen is characterized with 20% window opening ratio (OR) and its continuous and stiff RC floors. In order to elucidate the effect of W1, W2 and W3 weight loadings, the reference specimen was tested three times under W1, W2 and W3 using the same settlement profile.

4.1.1. Test 1 with W1

In this test, the reference specimen was tested under W1 weight loading. For this purpose, firstly RC blocks were placed onto the building floors by using mobile crane and then settlement effects were applied by deforming supporting IPE steel beams (tip displacement). Masonry walls significantly modified the applied settlement profile. A clear indication of this modification was the formation of gaps between wall bottom and steel beam. Around -45 mm tip displacement, at one of the corners of the building, a sudden damage occurred. Since the occurrence of this damage was attributed to a local imperfection regarding the masonry bed joint and workmanship in this region, this damage was not considered in the damage class evaluations. Figure 4.1 shows this damage in normal (a) and (b) close-up views. As seen, there was a major horizontal crack, and its width was around 20 mm (Crack 2 in Figure 4.2). The simultaneous inspections at -45 mm tip displacement revealed that there were also several cracks which were much thinner in width (Cracks 1, 3 and 4 in Figure 4.2).

(a) (b)

Figure 4.1. (a) The normal and (b) the close-up view of the local crack.

When the tip displacement went down to -65 mm (that was the reference maximum target tip displacement in the tests) no new crack appeared on any of the walls. Schematic views of parallel walls (with applied hogging profile) and cracks observed on their surfaces after Test 1 is demonstrated in Figure 4.2. Cracks were visible from both faces of the parallel front and back walls. Reference specimen had a significant rigid rotation. No new crack occurred even at -85 mm tip displacement. Following unloading (IPE steel beam was lifted back to its original horizontal position), the test setup was forced in upward direction (positive direction) to create a sagging settlement profile. It should be noted that sagging option was just for a trial and not used in other tests. When the tip displacement +30 mm (sagging), neither a new crack nor any plastic displacement (i.e. slippage of the walls over the IPE steel supports) occurred. During all these attempts the existing cracks either opened wider or closed.

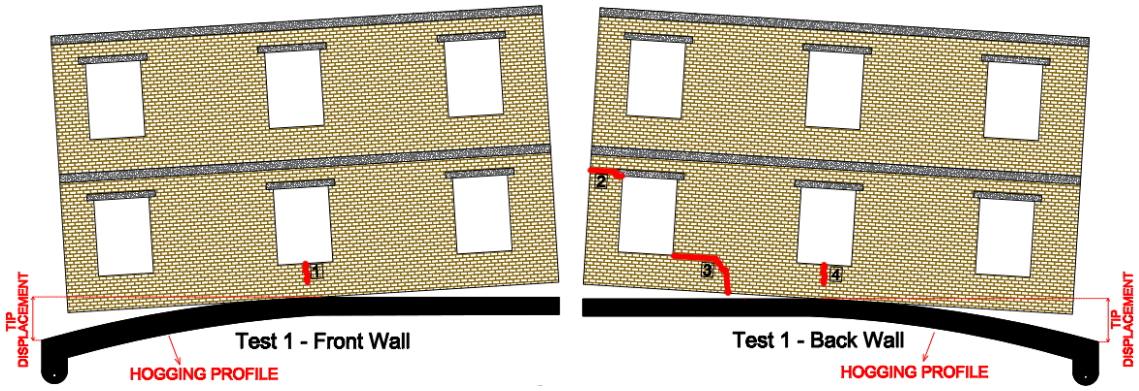

(a) (b)

Figure 4.2. Schematic views of parallel walls and cracks on their surfaces after Test 1: (a) front wall of the reference specimen, (b) back wall of the reference specimen.

Note that crack widths shown in Figure 4.2 were measured by using a crack ruler for both walls for the tip displacement of -66.89 mm. At this level, deflection ratio calculated based on the displacement data measured by DMS is 0.000215.

Damage class for front and back wall is determined based on the severity and number of existing cracks. Note that, inspected crack widths were multiplied by two due to geometrical scaling and compared with the crack width thresholds given in Table 2.2 to decide the damage class of the walls. For the tip displacement -66.89 mm, it is seen

that while damage class of front wall is slight (because of Crack 1), damage class of back wall is moderate (because of Crack 3 and Crack 4, Crack 2 was excluded from the evaluation).

Table 4.2. The deflection ratio value and maximum crack widths for tip displacement of -66.89 mm.

Δ/L at the end of the test (by DMS)	**Crack Line Number (Figure 4.2)**	**Maximum Crack Width for Each Crack Line (mm)**
0.000215	1	0.8
	2	20
	3	7.5
	4	0.15

4.1.2. Test 2 with W2

After Test 1 had been finalized, the weight loading was increased from W1 to W2. For this purpose, sandbags filled with barite aggregate (high density natural material) and plastic water tanks were placed onto the top and first floors.

In this test, the screw jack lowered down to -87 mm by exceeding the reference maximum tip displacement of -60 mm. In general, the existing cracks opened or closed. A thin crack in 0.6 mm width occurred on the front wall in addition to the existing cracks observed in Test 1. On the other hand, the gapping between front masonry wall and steel beam was about 25 mm. Figure 4.3 shows the gap opening. Note that no gap opening was observed for almost 1/3 of the wall length at the vicinity of the half length of the walls.

(a) (b)

Figure 4.3. Gapping occurred between reference building's front wall and steel beam: (a) general view, (b) close-up view.

At -87 mm tip displacement, the maximum gapping (between the steel beam and the wall) measured at the end of steel beam which is close to the point where screw jack operated was 25 mm. Figure 4.4 (a) and (b) show the schematic views of cracks of reference specimen's front and back walls after Test 2. Damages existed in Test 2 were also specified on these figures. Crack widths measured by using a crack ruler are presented for both walls for tip displacement of -89.24 mm in Table 4.3. At this level, deflection ratio calculated based on the displacement data measured by DMS is 0.000541. Damage class for front and back wall is determined based on the status of existing cracks using Table 2.2. For the tip displacement -89.24 mm, it is seen that while damage class of front wall is slight (because of Crack 1 and Crack 5), damage class of back wall is moderate (because of Crack 3 and Crack 4, Crack 2 was excluded from the evaluation).

Table 4.3. The deflection ratio value and maximum crack widths for tip displacement of -89.24 mm.

Δ/L at the end of the test (by DMS)	**Crack Line Number (Figure 4.3)**	**Maximum Crack Width for Each Crack Line (mm)**
0.000541	1	0.5
	2	15
	3	6
	4	0.12
	5	0.6

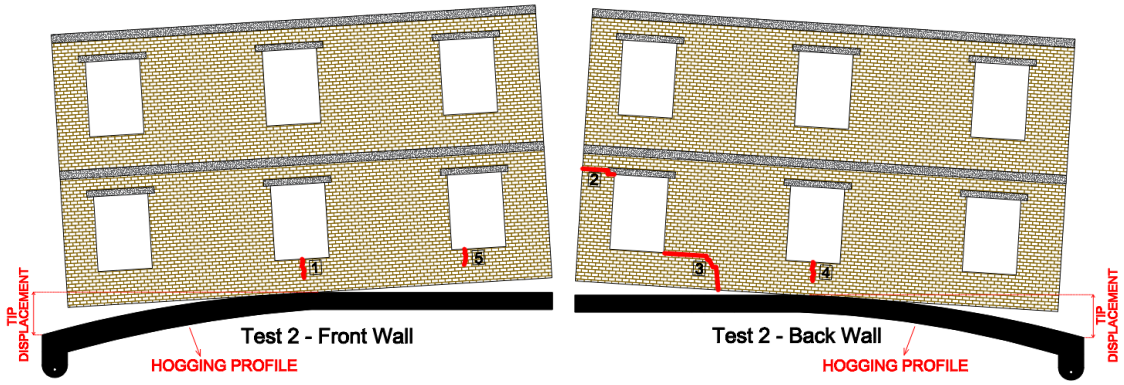

(a) (b)

Figure 4.4. Schematic views of walls and cracks after Test 2: (a) front wall of the reference specimen, (b) back wall of the reference specimen.

4.1.3. Test 3 with W3

Following Test 2, the weight loading was changed from W2 to W3. W3 is less than W2 in magnitude but the application of W3 is different. Since a part of weight loading was applied from ground floor windowsills (W3), the stress states change. Through window loading, an increase in total building weight can still be taken into account. However, window loading does not increase the normal compressive stress level at the sections above the bottom lines of the windows. This means that, these sections will be more prone to the tensile cracking and shear failure during settlement tests due to reduced normal compressive stress level.

In this test, the screw jack lowered down to -45 mm at maximum (maximum given tip displacement). During the test, at -14.5 mm tip displacement, new cracks 7, 8 and 9 appeared on the front wall. Figure 4.5 (a) and (b) show the schematic views of reference specimen's front and back walls at the end of Test 3. Crack 7 was the horizontal crack starting from upper left window corner and going through the pier and finishing at the edge of the wall. Cracks 8 and 9 were dominantly diagonal cracks but they started horizontally from bottom corners of the right and left windows at ground floor. At -23 mm tip displacement, cracks 10 and 13 were noticed. Crack 10 was observed at the front wall, it was a horizontal crack starting bottom right corner of the rightest window and

finishing at the edge of the wall. Crack 13 was at the back wall and its formation was the same with Crack 7. At -29.2 mm tip displacement, crack 6 and crack 12 were observed. Crack 6 was just upside of the second-floor slab, it was a horizontal crack. Crack 12 was at the back wall and its formation was the same with Cracks 8 and 9. At -32.1 mm tip displacement, Crack 11 was observed, and it was a dominantly horizontal crack starting from the upper window corner diagonally, going through the pier horizontally and finishing at the edge of the wall.

The test was stopped at -45 mm tip displacement due to safety concerns. However, DMS measurement could be recorded until the tip displacement of -34.94 mm.

The deflection ratio values and maximum crack widths (measured by a crack ruler) for tip displacement of -34.94 mm are presented in Table 4.4. Note that deflection ratio values were determined by processing DMS data. Figure 4.6 and 4.7 shows the wall damages and crack measurement technique after the completion of Test 3 before unloading.

Damage class for front and back wall is determined based on the severity and number of existing cracks using Table 2.2. For the tip displacement of -34.94 mm, it is seen that damage class of both front and back wall is severe (because of Cracks 1, 6, 7, 8, 9, 5, 10 and 11 for the front wall and because of Cracks 3, 4, 12 and 13 for the back wall. Crack 2 was excluded from the evaluation).

Table 4.4. The deflection ratio value and maximum crack widths for tip displacement of -34.94 mm.

Δ/L at the end of the test (by DMS)	**Crack Line Number (Figure 4.4)**	**Maximum Crack Width for Each Crack Line (mm)**
0.001753	1	0.5
	2	15
	3	6
	4	0.12
	5	0.11
	6	2
	7	10

	8	5
	9	5
	10	5
	11	7
	12	5
	13	10

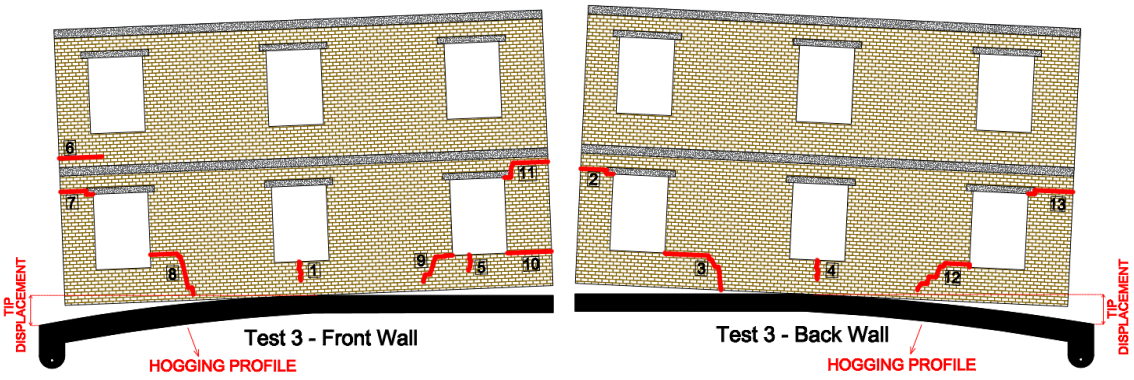

(a) (b)

Figure 4.5. Drawings of occurred cracks at the end of Test 3: (a) at the front wall of the reference specimen, (b) at the back wall of the reference specimen.

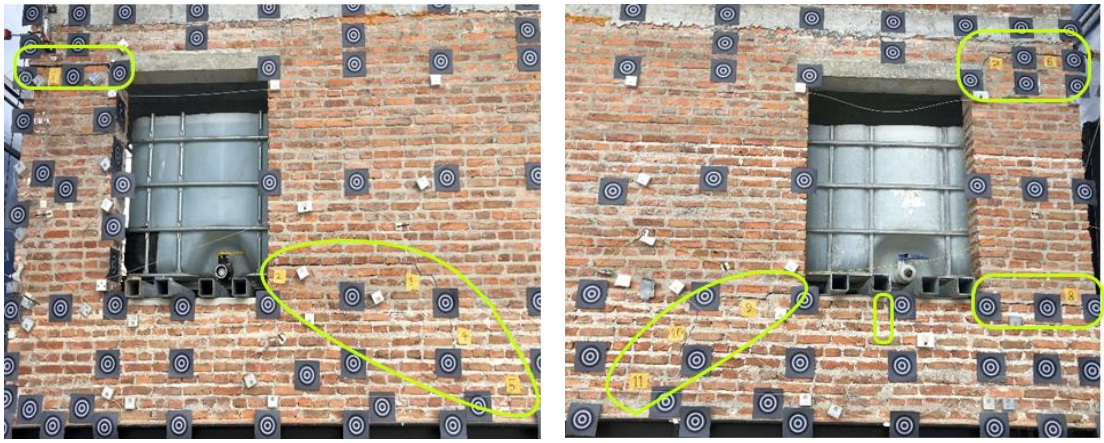

(a) (b)

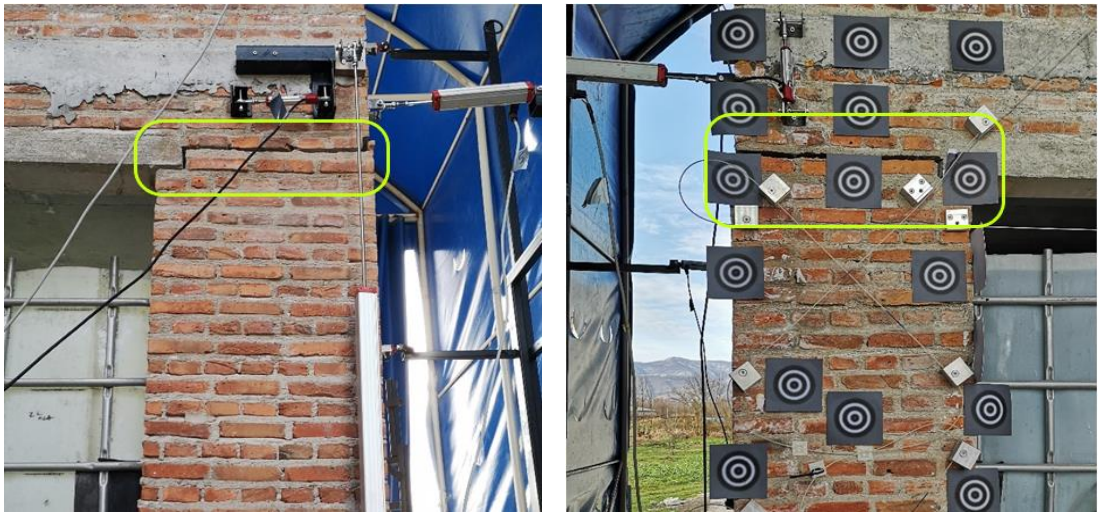

(c) (d)

Figure 4.6. Observed cracks after Test 3: (a) at the left part of the front wall, (b) at the right parts of the front wall, (c) at the top-right corner of the back wall, (d) at the top-left corner of the back wall.

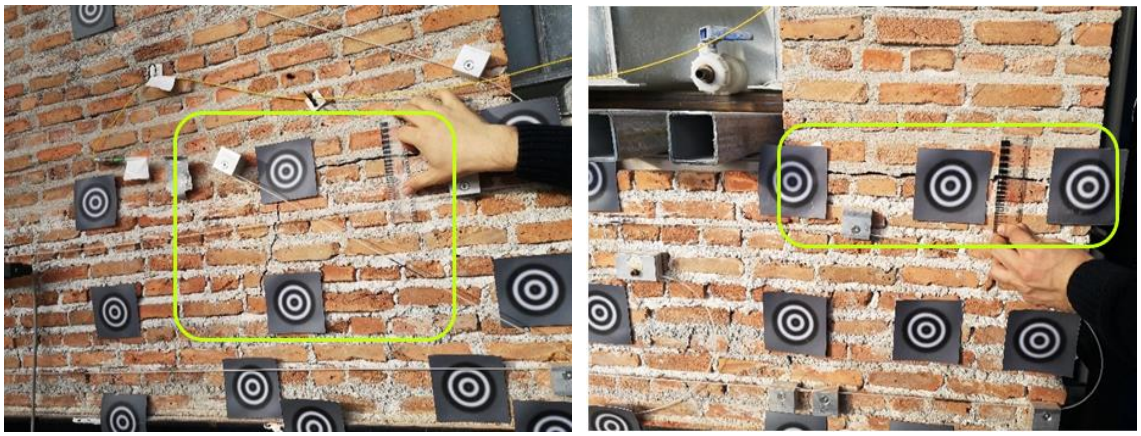

(a) (b)

Figure 4.7. Crack width is determined by crack ruler after Test 3: (a) for the middle part of the back wall and (b) for the bottom-right corner of the back wall.

4.2. Joist Floor Specimen Test (Test 4)

Joist floor specimen consisted of two parallel walls like other test specimens. However, its floor system was comprised of RC joists rather than of a continuous RC slab. These joists were located on the masonry walls at the second and first floor level.

They had 200 mm spacing through the length of the walls. Figure 4.8 shows assembled joists at the second floor and the first floor of the specimen. The absence of continuous slabs allowed this specimen to behave more flexible than specimens with continuous RC floors. Since the joists are located intermittently, they do not contribute to the flexural strength of the building in overall. RC joists have 120×150 mm (width×height) cross-section. They consisted of three steel rebars (φ8) at tension and compression sides and stirrups at every 100 mm along its length. The connection between the wall and RC joists for the first floor was done by using metal joist hangers. First, the hangers assembled to walls, then RC joists were mounted on these members. Lengths of joists were 1.65 m. Joist floor specimen had 20 % opening ratio in identical parallel walls.

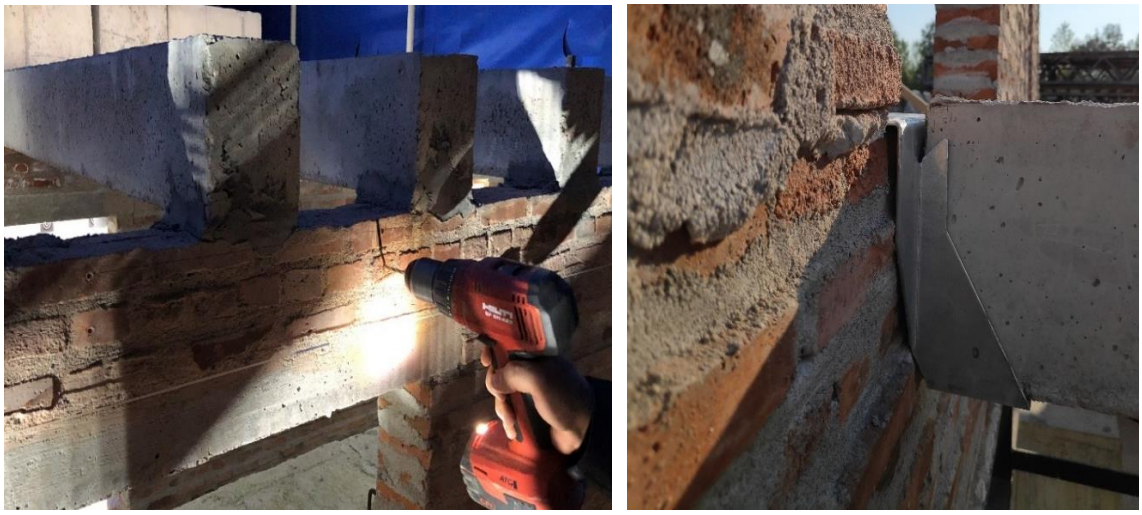

(a) (b)

Figure 4.8. Assembled joists: (a) at the top of the specimen, (b) at the first floor of the specimen.

4.2.1. Test 4 with W1

Joist floor specimen was tested only once using W1 weight loading scheme. At the initial steps of the settlement test, gap formation between walls and IPE steel beams was observed. At -30 mm tip displacement, a quite brittle splitting developed loudly. All the measurement systems recorded the building damage. The width of the vertical cracks

was larger toward the top of the walls. On the other hand, all of them occurred in a region that was almost 1/3 of the entire wall length on the middle. These observations supported that the bending moments were the governing factor of such a damage. Since there were no continuous RC slabs, the cracks could initiate at the top and they traveled between the stories.

Figure 4.9 (a) and (b) show the schematic views of joist floor specimen's front and back walls after Test 4. The deflection ratio value and maximum crack widths for tip displacement of -32.12 mm are presented in Table 4.5. Note that deflection ratio value was determined by processing DMS data for front wall only. Figure 4.10 shows the wall damages after the completion of Test 4 before unloading. Damage class of both walls decided based on the Table 2.2 was very severe.

Table 4.5. The deflection ratio value and maximum crack widths for tip displacement of -32.12 mm.

Δ/L at the end of the test (by DMS)	**Crack Line Number (Figure 4.7)**	**Maximum Crack Width for Each Crack Line (mm)**
0.002484	1	10
	2	32
	3	22
	4	5
	5	36
	6	8
	7	21
	8	12
	9	3

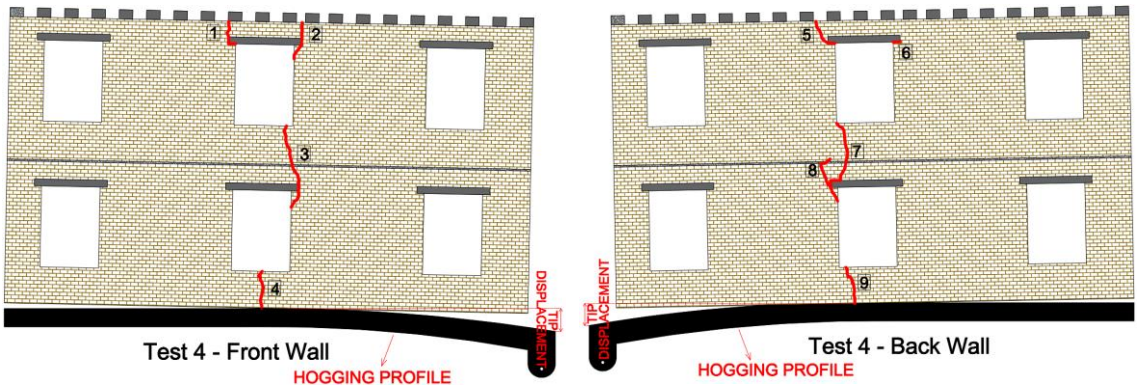

(a) (b)

Figure 4.9. Schematic views of cracks occurred at the end of Test 4: (a) at the front wall of the joist floor, (b) at the back wall of the joist floor.

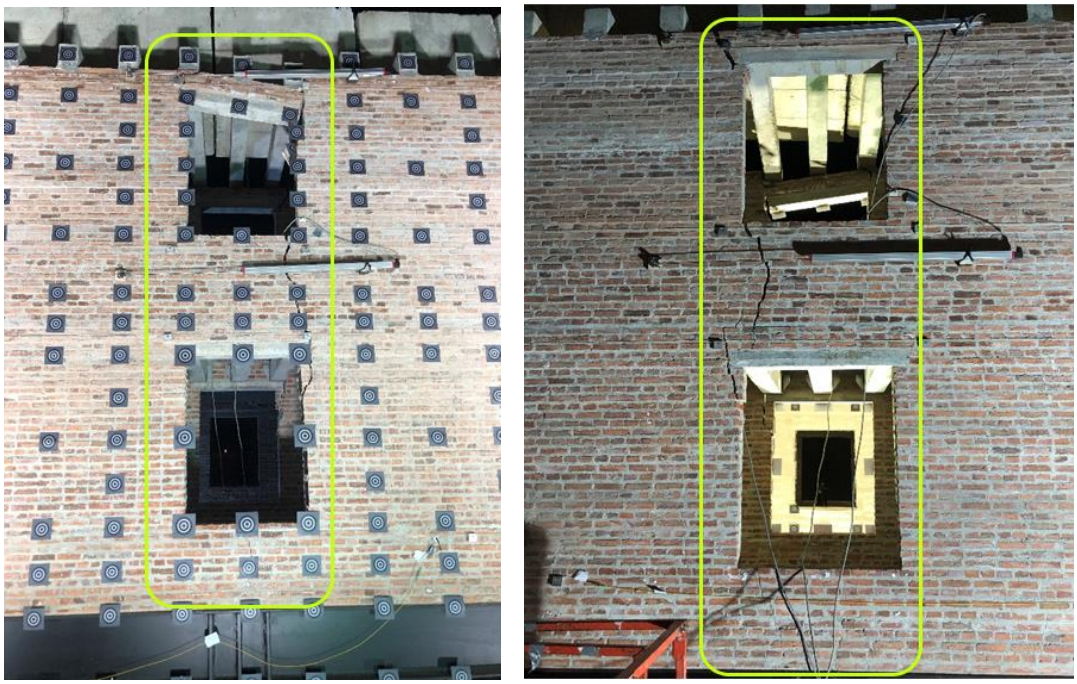

(a) (b)

Figure 4.10. Observed cracks after Test 4: (a) at the front wall of the joist floor specimen and (b) at the back wall of the joist floor specimen.

4.3. Combined Specimen Test (Test 5)

Combined specimen consisted of parallel masonry walls with and without window openings. While one of the walls had five window openings (35% OR) (perforated wall), at each storey, the other wall did not have any window opening (blind wall). This specimen was specifically designed to examine the effect of different ORs on the settlement response. Floor type of this specimen was continuous and rigid. Combined specimen was tested under W1 weight loading using the same pre-defined settlement profile.

4.3.1. Test 5 with W1

When the test started, gap formation between front/back masonry walls and steel IPE beams was observed. However, unlike the other specimens having identical parallel

walls, the gapping did not develop at the same rate for perforated and blind walls. While gapping increased constantly for blind wall, it remained much more limited for perforated wall. This was a clear sign of that blind wall modified the applied settlement profile due to its stiffness. On the other hand, perforated wall was much more flexible due to large window openings and tended to conform to the applied settlement profile more closely. This also means that perforated wall did experience more severe damage.

During Test 5, while slight to moderate level of cracks occurred for perforated wall, no cracking was observed for blind wall. Around -17 mm tip displacement, for perforated wall, the thickness of the horizontal cracks at the top of the most right and most left piers were about 3 mm in width. Around -25 mm tip displacement, the test was stopped due to safety concerns.

The deflection ratio and maximum crack widths for tip displacement of -25.93 mm are presented in Table 4.6. Note that deflection ratio value was determined by processing DMS data. Figure 4.11 demonstrates the crack pattern observed at the end of the Test 5: (a) on the front wall (perforated wall) and, (b) on the back wall (no-opening wall). Figure 4.12 shows the wall damages before unloading. Damage class of the front wall decided based on the Table 2.2 was moderate.

Table 4.6. The deflection ratio value and maximum crack widths for tip displacement of -25.93 mm.

Δ/L at the end of the test (by DMS)	**Crack Line Number (Figure 4.9)**	**Maximum Crack Width for Each Crack Line (mm)**
0.001346	1	3
	2	1
	3	0.2
	4	0.35
	5	0.65
	6	1.5
	7	4.5

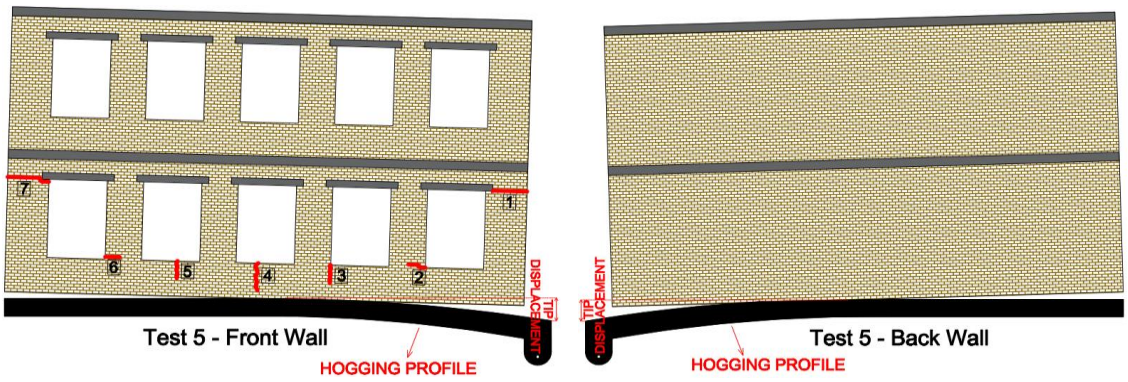

(a) (b)

Figure 4.11. Drawings of cracks occurred at the end of Test 5: (a) on the front wall (perforated wall) of the combined specimen, (b) on the back wall (no-opening wall) of the combined specimen.

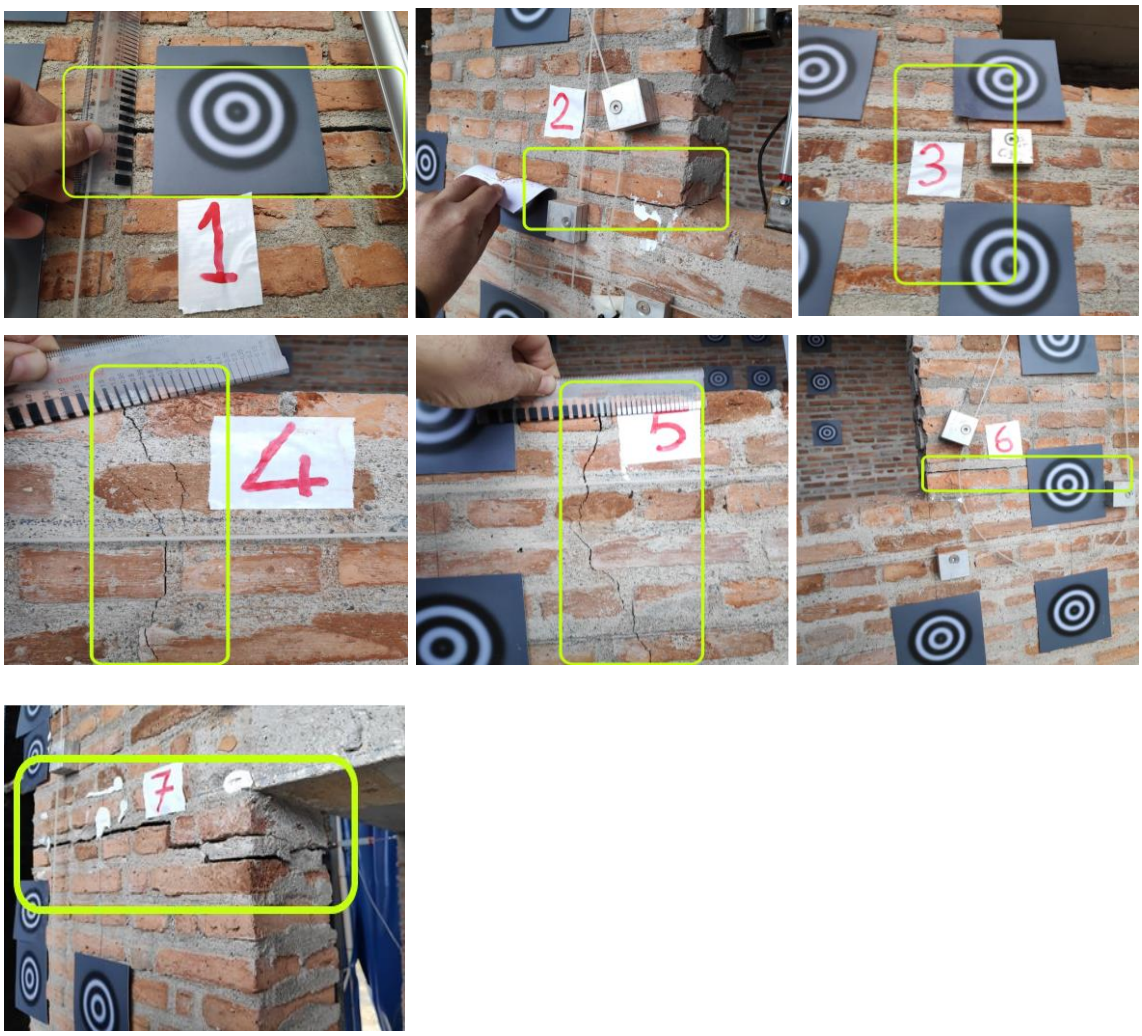

Figure 4.12. Cracks occurred on the combined specimen at the end of Test 5.

4.4. Evaluation of the Main Test Observations

In this sub-section, an evaluation for the main test observations is presented for three building wall specimens tested using the pre-defined settlement profiles. Although the initial plan was to reach/apply the same target tip displacement for all the specimens, it could not be possible because of the extent of the damages developed and safety concerns. Specimens possessed different features varying from floor type to window opening ratio and the weight.

For many of the specimens, the gap formation between the IPE steel beams and the masonry walls is very pronounced, indicating that those specimens significantly modify the applied settlement profile. The weight of the building has a reducing effect on this.

Floor type is a very effective parameter. It is seen that the specimens with stiff and continuous floors modifies the applied settlements in the maximum extent. The largest gap formation was observed in such buildings. However, when the position of the weight loading was changed (loading through ground floor windowsills), the stress states on the walls also changed. While higher vertical compressive stresses were effective on the walls due to the weight loads placed on the floors in the first attempts, when some of the loads were applied through the windowsills near to the bottom of the walls, a decrease in the initial compressive stress level occurred in the upper parts of the ground floor. This facilitated the formation of horizontal and diagonal cracks in nearby sections due to the increasing effectiveness of the tensile stresses. Except for Joist floor specimen, almost all of the cracks occurred on the ground floor walls of building specimens. From this aspect, it can be interpreted that the presence of the continuous floor diminished the settlement effects on the second floor and decreased the distortions to propagate from one story to another.

An unexpected local crack (Crack 2) occurred at the back wall of the reference specimen in Test 1. The occurrence of this crack can be explained by the presence of some imperfection regarding masonry material, bond properties of mortar and workmanship. Undoubtedly, the effect of this failure to the other tests of this specimen (Test 2 and Test 3) could not be zero, but both in preliminary numerical analyses and in testing process it was seen that this effect did not take a big role on the behavior of the

other wall (front wall) of the reference specimen. Damage pattern of the front wall occurred as it should be and almost independently from the back wall that had the local crack. Therefore, it can be assumed that however parallel walls of specimens are connected to each other by slabs, they can response to a given tip displacement, individually. This assumption can be confirmed by the result of Combined Specimen Test (Test 5), as well. Despite there was a considerable stiffness difference between the parallel walls of this specimen (perforated wall and blind wall), each wall could reveal their individual response distinctly.

The joist floor building is the specimen that behaves most conforming with the applied settlement profile. The absence of continuous slabs allowed this specimen to behave more flexibly. It can be interpreted that in the absence of strong diaphragms, the behavior of buildings with wooden floors would be formed in this way. During the settlement tests, wide and sudden cracks occurred from the top down on both parallel walls at relatively low tip displacement steps.

Deflection ratio values could be calculated for only front walls since only those walls could be monitored by DMS. Deflection ratio values calculated based on the monitored data are consistent with the flexibility of the specimens. In this regard, the maximum deflection ratio was calculated for Joist floor specimen. In overall, as the deflection ratio increases the observed damage class of the specimens increases.

CHAPTER 5

ANALYTICAL CALCULATIONS

5.1. Introduction

In this chapter, experimental test results are compared to the predictions made by the LTSM. As the details are explained in Chapter 2, LTSM adopts a fictitious beam approach to calculate the maximum average tensile strains within the buildings subjected to excavation-induced ground displacements. Based on the magnitude of calculated strains, potential settlement damage class is determined. Several researchers suggested different expressions to take the building stiffness into account in calculations. In this study, the stiffness relations suggested by Potts and Addenbrooke (1997) and Melis and Rodriguez Ortiz (2001) were adopted. Besides, extrapolations were made based on the Son and Cording (2007) to estimate the most appropriate values of *E/G* for varying window opening ratios.

5.1.1. Equivalent Bending Stiffness Relations for Buildings

Potts and Addenbrooke (1997) put forward the following relation to calculate the equivalent bending stiffness of the building:

$$EI = E \sum_{i=1}^{n+1} I_{slab,i} + A_{slab,i} \times d_i^2 \quad (5.1)$$

where *E* is the elastic modulus of floor slabs, *i* is the number of floor slabs, n is the number of storeys, $I_{slab,i}$ is the second moment of inertia of each slab, $A_{slab,i}$ is the cross-sectional area of each slab and d_i is the vertical distance between the neutral axis of the structure and the neutral axis of the slab. As seen, this relation accounts for the bending stiffness contribution of only floor slabs and depends on the parallel axis theorem.

Whereas Melis and Rodriguez Ortiz (2001) suggested a unified approach considering the contributions of slabs, load-bearing masonry walls and the basement:

$$EI = \sum(EI)_{floors} + \sum(EI)_{walls} + \sum(EI)_{basements} \quad (5.2)$$

where $(EI)_{floors} = E(\frac{1}{12}Bb_s^3 + Bb_s d_s^2)\frac{1}{B}$ is the contribution of each floor slab, $(EI)_{walls} = E(\frac{1}{12}b_w H^3 + b_w H d_w^2)\frac{1}{B}$ is the contribution of each wall and $(EI)_{basements} = E(\frac{1}{12}Bb_b^3 + Bb_b d_b^2)\frac{1}{B}$ is the contribution of each foundation slab rigidly connected to the superstructure. In these equations, *H* is the total height of the building, *B* is the width of the specimen which is parallel to the tunneling line, b_s is the slab thickness, b_w is the wall thickness, d_s is the vertical distance between the neutral axis of the structure and the neutral axis of the slab, d_w is the vertical distance between the neutral axis of the structure and the neutral axis of the wall and d_b is the vertical distance between the neutral axis of the structure and the neutral axis of the basement. The second moment of area of each slab is neglected with respect to its own middle plane. Additionally, because of their reduced stiffness, partition walls are neglected. In the current study, bending stiffness of basement is zero because there is no actual foundation for the test specimens. It should also be noted that Melis and Rodriguez Ortiz (2001) includes the reduction factors to take into account the effect of door and window openings on the calculated stiffness values. They suggest the reduction factors which are dependent on the percentage of openings and the aspect ratio of the structure (shown in the next sections in Table 5.10).

This chapter presents five different calculations to obtain the maximum tensile strain values for each of test specimens (reference, joist floor and combined wall specimens) with different opening ratios.

Calculation 1 includes the application of the classical LTSM which was developed by Burland and Wroth (1974). In this calculation, all assumptions of these researchers were followed. The second moment of inertia was taken as $I = 1x\ H^3/12$ for hogging case, Poisson's ratio was taken as 0.3, therefore E/G value was taken as 2.6 for all specimens by not considering opening ratio (*OR*).

Calculation 2 includes the application of the LTSM again (developed by Burland and Wroth, 1974). However, in this calculation, the different values of *E/G* were adopted based on the suggestions of Son and Cording (2007).

Calculation 3 includes the application of equivalent bending stiffness relations of Melis and Rodriguez Ortiz (2001). In this study, the shear modulus (G) is obtained by $E/G = 2 \times (1 + \nu)$. Poisson's ratio (ν) was taken as 0.3. The stiffness values are also reduced based on the reduction factors suggested by Melis and Rodriguez Ortiz (2001). Calculated reduced stiffness values are incorporated with the LTSM (beam approach and damage class determination) proposed by Burland and Wroth (1974).

Calculation 4 includes equivalent bending stiffness relation of Potts and Addenbrooke (1997). Since the walls are not accounted in their stiffness calculations no reduction factors are applicable for different wall openings. Calculated reduced stiffness values are incorporated with the LTSM (beam approach and damage class determination) proposed by Burland and Wroth (1974).

Calculation 5 includes the application of equivalent bending stiffness relations of Melis and Rodriguez Ortiz (2001). However, different from the Calculation 3, reduction is made for only stiffness contribution of the masonry walls. The bending stiffness contribution of slabs is not reduced and directly added to the reduced wall stiffness values.

Calculation 6 is another derivation for Melis and Rodriguez Ortiz (2001). In this last calculation, the stiffness contribution of slabs is totally omitted. The equivalent bending stiffness is calculated based on the reduced contribution of the masonry walls.

5.2. Calculation 1: Classical application of beam approach by Burland and Wroth (1974)

Herein, test specimens were considered as simply supported beams. They are in a hogging zone. Because of this reason, the neutral axis of the system was assumed as being along the bottom edge, so the value of neutral axis depth (t) became equal to height of the structure. Then, the second moment of inertia (I) of the structure was calculated according to the location of the neutral axis as $H^3/3$. Based on the results of the preliminary numerical analyses, the modulus of elasticity of the masonry walls was considered as 3300000 KPa. Burland and Wroth (1974) proposed E/G=2.6 for massive masonry walls. Thus, E/G ratio was taken for all walls (except perforated wall of the combined specimen) as 2.6. Burland and Wroth (1974) suggested E/G=12.5 for very flexible structures.

Therefore, for perforated wall, ratio of E/G was taken as 12.5. When the Equation (2.6) and the Equation (2.7) were used, the strain values for bending critical case and for shear critical case were found, respectively (presented in Chapter 6). Table 5.1 shows the input values that were used in the LTSM calculations for both bending and shear critical cases.

Table 5.1. Input values that were used in the LTSM calculations (for both bending and shear critical cases).

Input Values – for both Bending and Shear Critical Cases in Hogging								
Wall OR	**L (m)**	**H (m)**	**t (m)**	**E (kPa)**	**E/G ratio**	**G (kPa)**	**I (m^4)**	**EI (kNm^2)**
For all type of openings (0%, 20% and 35%)	5,6	3,2	3,2	3300000	2,6	1269231	10,92267	36044811

5.3. Calculation 2: Application of beam approach with E/G ratios derived according to Son and Cording (2007)

In Calculation 2, to modify the E/G ratio for different types of walls, suggestions of Son and Cording were followed. Herein, E/G ratios of building specimens which had different opening ratios were determined by using interpolations according to suggestions of Son and Cording (2007). By the help of interpolations, E/G ratio for the walls which had 20% OR (reference and joist floor building specimens) was found as 9.5 and E/G ratio for the walls which had 35% OR (perforated wall of combined building specimen) was found as 12.5. When the Equation (2.6) and the Equation (2.7) was used, the strain values for bending critical case and for shear critical case were found, respectively (presented in Chapter 6). Inputs values that were used for both bending and shear critical cases in LTSM is shown in Table 5.2.

Table 5.2. Input values that were used in the LTSM calculations (for both bending and shear critical cases).

Input Values – for both Bending and Shear Critical Cases in Hogging								
Wall OR	**L (m)**	**H (m)**	**t (m)**	**E (kPa)**	**E/G ratio**	**G (kPa)**	**I (m^4)**	**EI (kNm^2)**
0% (No Opening blind wall)	5,6	3,2	3,2	3300000	2,6	1269231	10,92267	36044811
20% (3-Openings)	5,6	3,2	3,2	3300000	9,5	347368,4	10,92267	36044811
35% (5-Openings)	5,6	3,2	3,2	3300000	12,5	264000	10,92267	36044811

5.4. Calculation 3: Application of beam approach using the equivalent bending stiffness and stiffness reduction concepts of Melis and Rodriguez Ortiz (2001)

In Calculation 3, building bending stiffness calculations were performed according to unified approach that was developed by Melis and Rodriguez Ortiz (2001). In addition, reduction factors proposed by the same researchers were also used to better estimate the building bending stiffness values. As seen in Table 5.3, the reduction factors are determined based on the type of the wall and specimen length/height ratio. For all the specimens, L/H is 1.75, which was smaller than 2. Thus, the case of L<2H case was considered. For, 0%, 20% and 35% opening ratios, reduction factors are as follows:

- 0% → R.F=1
- 20% → R.F=0.4
- 35% → R.F=0.1

Table 5.3. Reduction factors on building bending stiffness (EI) due to openings. (Source: Melis and Rodriguez Ortiz, 2001)

Type of wall	Length<2H	Length>2H
No openings	1.00	1.00
Openings from 0 to 15%	0.70	0.90
Openings from 15 to 25%	0.40	0.60
Openings from 25 to 40%	0.10	0.15

For the modulus of elasticity (E) of masonry wall, 3300000 kPa is considered. Then, by using $G = E/(2 * (1 + \nu))$ formula, which is suggested by Burland and Wroth (1974), G is found as 1269230,8 kPa. As mentioned in Section 2.3.2, E is the elasticity modulus, G is the shear modulus, ν is the Poisson's ratio which was taken as 0.3. In the light of suggestions of Melis and Rodriguez Ortiz (2001), the total bending stiffness of building specimens with stiff floor (reference and combined building specimens) is found as 6176406,7 kPa. However, because of the absence of a continuous stiff floor of joist floor building, the total bending stiffness of this specimen is equal to the total bending stiffness of walls (2075073,4 kPa).

Using the reduction factors calculated based on the wall opening ratio and length to height relationship (L<2H for the current specimens), bending stiffness values are reduced as shown in Table 5.4. By using reduced total bending stiffness values, LTSM is applied for each specimen. Input values that were used in the LTSM for both bending and shear critical cases is shown in Table 5.5.

Table 5.4. Reduced building bending stiffness values for L<2H.

Wall	**Opening Ratio**	**Reduction Factor**	**$\sum$(EI) (reduced) (kNm^2)**
No opening (Blind wall)	0%	1	6176406,7
3-openings (Reference)	20%	0,4	2470562,7
3-openings (Walls of Joist Floor Building)	20%	0,4	830029,4
5-openings (Perforated wall)	35%	0,1	617640,7

Table 5.5. Input values that were used in the LTSM calculations (for both bending and shear critical cases).

Input Values – for both Bending and Shear Critical Cases in Hogging							
Wall	**L (m)**	**H (m)**	**t (m)**	**$\sum$(EI) (reduced) (kNm^2)**	**G (kPa)**	**EI/G (m^4)**	**G/EI (1/m^4)**
No opening (Blind wall)	5,6	3,2	3,2	6176406,7	1269230,8	4,8663	0,2055
3-openings (Reference)	5,6	3,2	3,2	2470562,7	1269230,8	1,9465	0,5137
3-openings (Walls of Joist Floor Building)	5,6	3,2	3,2	830029,4	1269230,8	0,6539	1,5291
5-openings (Perforated wall)	5,6	3,2	3,2	617640,7	1269230,8	0,4866	2,0549

5.5. Calculation 4: Application of beam approach using the equivalent bending stiffness relation of Potts and Addenbrooke (1997)

Calculation 4 is performed according to proposals of Potts and Addenbrooke (1997) about building bending stiffness. After finding the building bending stiffness, LTSM is used. In the calculation of building bending stiffness, they consider the contribution of only floors. When the necessary calculations are performed, the total bending stiffness of floors is found as 4101333,33 kNm^2. In this study, the modulus of elasticity (E) of RC slabs are considered as 32000000 kPa, and shear modulus (G) is found

as 12307692,31 kPa by using $E/G = (2 \times (1 + \nu))$ formula. Other input values that were used in LTSM are provided in Table 5.6.

Table 5.6. Input values that were used in the LTSM calculations (for both bending and shear critical cases).

Input Values – for both Bending and Shear Critical Cases in Hogging							
L (m)	**H (m)**	**t (m)**	**E (kPa)**	**G (kPa)**	**∑(EI)floors (kNm²)**	**EI/G (m⁴)**	**G/EI (1/m⁴)**
5,6	3,2	3,2	32000000	12307692,31	4101333,33	0,3332	3

5.6. Calculation 5: Application of beam approach using the equivalent bending stiffness concept of Melis and Rodriguez Ortiz (2001) – no stiffness reduction for slabs

The difference of Calculation 5 from Calculation 3 is simply that reduction factors were applied only on total bending stiffness value of the walls. Then, these reduced stiffness values for walls which had different opening ratios were summed with the total bending stiffness of floors to find the overall reduced bending stiffness of building. Equation (5.3) below explains the partial stiffness reduction concept:

$$\sum(EI)_{(partially\ reduced)} = \sum(EI)_{walls\ (reduced)} + \sum(EI)_{floors} \quad (5.3)$$

Modulus of elasticity (*E*) is selected as 3300000 kPa for masonry walls. By the help of elasticity theory, shear modulus (*G*) is found as 1269230,8 kPa. At first, total bending stiffness values of all walls is equal to 2075073,4 kPa, because they have same dimensions. Stiffness contribution of floors (for reference and combined specimen) are found as 4101333,3 kPa. Therefore, the total bending stiffness of building specimens with stiff floor (reference and combined specimens) are found as 6176406,7. In addition, because of the absence of a continuous stiff floor of joist floor building, the total bending stiffness of this specimen is equal to the total bending stiffness of walls (2075073,4 kPa).

Using the reduction factors calculated based on the wall opening ratio and length to height relationship (L<2H for the current specimens), partially reduced building bending stiffness values are shown in Table 5.7.

Table 5.7. Partially reduced building bending stiffness values for L<2H.

Wall	Opening Ratio	Reduction Factor	∑(EI)walls(reduced) (kNm²)	∑(EI)floors (kNm²)	∑(EI)(partially reduced) (kNm²)
No opening (Blind wall)	0%	1	2075073,4	4101333,3	6176406,7
3-openings (Reference)	20%	0,4	830029,4	4101333,3	4931362,7
3-openings (Walls of Joist Floor Building)	20%	0,4	830029,4	0	830029,4
5-openings (Perforated wall)	35%	0,1	207507,34	4101333,3	4308840,7

By using partially reduced bending stiffness values, LTSM is applied for each specimen. Input values that were used in the LTSM for both bending and shear critical cases is shown in Table 5.8.

Table 5.8. Input values that were used in the LTSM calculations (for both bending and shear critical cases).

Input Values – for both Bending and Shear Critical Cases in Hogging							
Wall	L (m)	H (m)	t (m)	∑(EI) (partially reduced) (kNm²)	G (kPa)	EI/G (m⁴)	G/EI (1/m⁴)
No opening (Blind wall)	5,6	3,2	3,2	6176406,749	1269230,8	4,8663	0,2055
3-openings (Reference)	5,6	3,2	3,2	4931362,70	1269230,8	3,8853	0,2574
3-openings (Walls of Joist Floor Building)	5,6	3,2	3,2	830029,4	1269230,8	0,6539	1,5291
5-openings (Perforated wall)	5,6	3,2	3,2	4308840,67	1269230,8	3,3948	0,2946

5.7. Calculation 6: Application of beam approach using the equivalent bending stiffness concept of Melis and Rodriguez Ortiz (2001) – no slab contribution

In Calculation 6, equivalent bending stiffness concept of Melis and Rodriguez Ortiz (2001) is adopted. However, different from the previous iterations made on the original equivalent stiffness concept of these authors, this time the contribution of slabs is totally disregarded. Equation (5.4) below explains the partial stiffness reduction concept:

$$\sum(EI)_{(reduced)} = \sum(EI)_{walls\ (reduced)} \tag{5.4}$$

Then, LTSM is applied to all specimens. It should be noted that since there is no consideration of the effects of floors to bending stiffness, building bending stiffness values of joisted floor and reference specimen is equal. Because they both have similar wall configurations with 3-openings. Table 5.9 demonstrates building bending stiffness values calculated and reduced according to proposals of Melis and Rodriguez Ortiz (2001).

Table 5.9. Partially reduced building bending stiffness values for L<2H.

Wall	**Opening Ratio**	**Reduction Factor**	**$\sum$(EI)walls $_{(reduced)}$ (kNm^2)**	**$\sum$(EI)floors (kNm^2)**	**$\sum$(EI) $_{(reduced)}$ (kNm^2)**
No opening	0%	1	2075073,415	0	2075073,415
3-openings	20%	0,4	830029,366	0	830029,366
5-openings	35%	0,1	207507,342	0	207507,342

By using reduced total bending stiffness values in Table 5.9, LTSM is applied for each specimen. Input values that were used in LTSM is shown in Table 5.10.

Table 5.10. Input values that were used in the LTSM calculations (for both bending and shear critical cases).

Input Values – for both Bending and Shear Critical Cases in Hogging							
Wall	**L (m)**	**H (m)**	**t (m)**	**$\sum$(EI)walls $_{(reduced)}$ (kNm^2)**	**G (kPa)**	**EI/G (m^4)**	**G/EI (1/m^4)**
No opening	5,6	3,2	3,2	2075073,415	1269230,8	1,6349	0,6117
3-openings	5,6	3,2	3,2	830029,366	1269230,8	0,6539	1,5291
5-openings	5,6	3,2	3,2	207507,342	1269230,8	0,1635	6,1166

CHAPTER 6

RESULTS

This chapter compares the results of analytical calculations with the experimental results. Tables are used to present the calculation method, deflection ratio (Δ/L), calculated maximum tensile strain (ε_{bmax} or ε_{dmax}), predicted damage class (obtained through LTSM) and observed damage class (determined based on measured in-situ crack widths) of the specimens. Damage class predictions were made by comparing calculated maximum tensile strain values with the limiting tensile strain intervals presented in Table 2.2. It should be noted that only one of the parallel walls (always named as front wall in this thesis) could be monitored by DMS. This means that deflection ratio could be determined for only front walls. Therefore, damage class of each building specimen is assessed based on the results of front walls only. This does not usually address a problem because all the building specimens (except for combined wall building specimen) revealed similar damage patterns for both walls. On the other hand, recall that only front wall (perforated wall) of combined wall building specimen had visible damage. Damage class of combined wall building specimen is determined based on the damages on the front wall, only.

These comparisons are useful to evaluate the accuracy of the LTSM, which was incorporated with different equivalent stiffness relations, in predicting actual damage class (determined in Chapter 4 based on the inspected max. crack width) of each specimen tested.

For convenience of the comparisons, Table 6.1 presents a summary of the calculation methods presented in Section 5.

Table 6.1. Summary of the features of calculation methods presented in Section 5.

CALCULATION ID	DESCRIPTION	PROPOSED BY / MODIFIED FROM
1	* Original LTSM * E/G ratio was taken as 2.6 for all specimens	* Burland and Wroth (1974)

2	* LTSM * E/G ratio was determined based on interpolation	* Burland and Wroth (1974) * Son and Cording (2007)
3	* LTSM * Stiffness calculations for slabs and walls * Total bending stiffness is reduced by reduction factors	* Burland and Wroth (1974) * Melis and Rodriguez Ortiz (2001)
4	* LTSM * Stiffness calculations for slabs	* Burland and Wroth (1974) * Potts and Addenbrooke (1997)
5	* LTSM * Stiffness calculations for slabs and walls * Only the total bending stiffness of walls is reduced by reduction factors	* Burland and Wroth (1974) * Modified from Melis and Rodriguez Ortiz (2001)
6	* LTSM * Stiffness calculations only for walls * Only the total bending stiffness of walls is reduced by reduction factors	* Burland and Wroth (1974) * Modified from Melis and Rodriguez Ortiz (2001)

6.1. Results for Reference Specimen (Test 1, Test 2 And Test 3)

6.1.1. Test 1

The maximum crack width of the front wall was 0.8 mm (1.6 mm in full size building) at the end of the Test 1. Based on this crack width, actual damage class of this building is determined as slight. Table 6.2 presents the damage classes calculated by LTSM using different stiffness relations. As seen, Calculations 3, 4, 5 and 6 can estimate actual the front wall damage accurately as slight. However, Calculation 1 and Calculation 2 underestimate the actual damage class. This is because of the fact that the magnitude of building stiffness considered in the Calculations 1 and 2 is larger than that considered in the Calculations 3-6. As building stiffness gets higher, calculated maximum tensile strain values become less.

Note that, for Calculation 2, E/G ratio was taken as 9.5, as showed in Chapter 5 for OR=20%.

Table 6.2. Analytical results of Test 1.

Calculation	Δ/L	Ɛbmax (%)	Ɛdmax (%)	Damage Class obtained by LTSM	Actual Damage Class obtained by tests [Front Wall (DMS aspect)]
1	0,000215	0,0242	0,0179	Very Slight	Slight
2	0,000215	0,0075	0,0204	Negligible	
3	0,000215	0,1093	0,0056	Slight	
4	0,000215	0,1391	0,0012	Slight	
5	0,000215	0,0869	0,0088	Slight	
6	0,000215	0,1319	0,0023	Slight	

Unlike the general trend in the analytical predictions shown in Table 6.2, for Calculation 2, maximum diagonal (shear) tensile strain (ε_{dmax}) is greater than the maximum bending tensile strain (ε_{bmax}). The reason of this is to account for an E/G ratio bigger than 2.6 in the calculations. For the ranges L/H<2 and E/G >2.6, the classical beam approach estimates that diagonal tension is more critical (decisive) than bending. Dalgic et al. (2018) express this tendency in their paper as well. As shown in Figure 6.1, each composite curve shows the relationship between L/H and $(\Delta/L)/\varepsilon_{max}$ values for hogging. The kink points on these curves specify the transition points from shear to bending critical cases of the wall structures. Note that how shear critical range of L/H expands when a higher value of E/G ratio is chosen. This figure also explains why Calculation 1 (E/G=2.6) points out relatively higher damage class (Very slight) than the Calculation 2 (E/G=9.5) (Negligible). For L/H<2 and a given Δ/L, the curves for E/G >2.6 corresponds to a higher $(\Delta/L)/\varepsilon_{max}$ value that eventually leads to smaller maximum tensile strains (ε_{max}) and lower damage classes, accordingly. This fact regarding Calculations 1 and 2 is also valid for the following assessments made in this section.

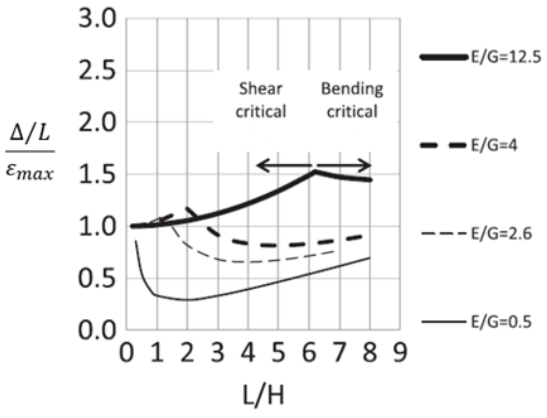

Figure 6.1. $\frac{\Delta/L}{\varepsilon max}$ – L/H composite curves obtained for different values of E/G for hogging.

6.1.2. Test 2

The maximum crack width was 0.6 mm (1.2 mm in full size building) on the front wall. Based on this, the actual damage class for the front wall is slight. As seen in Table 6.3, damage classes calculated by LTSM using Calculations 3, 4, 5 and 6 overestimate the front wall damage. Calculation 1 and Calculation 2 underestimate the front wall damage. As mentioned in Chapter 5, E/G ratio was taken as 9.5 for Calculation 2 (OR=20%).

Table 6.3. Analytical results of Test 2.

Calculation	Δ/L	Ɛbmax (%)	Ɛdmax (%)	Damage Class obtained by LTSM	Actual Damage Class obtained by tests [Front Wall (DMS aspect)]
1	0,000541	0,0609	0,0452	Very Slight	Slight
2	0,000541	0,0189	0,0513	Very slight	
3	0,000541	0,2749	0,0140	Moderate	
4	0,000541	0,3501	0,0031	Severe	
5	0,000541	0,2186	0,0222	Moderate	
6	0,000541	0,3320	0,0057	Severe	

6.1.3. Test 3

The maximum crack width of the front wall was 10 mm (20 mm in full size building) Based on this, actual damage for front wall of this specimen were severe. As seen in Table 6.4, damage classes calculated by LTSM using Calculations 3, 4, 5 and 6 overestimate the front wall damage. Stiffness reductions based on the ratio of the window openings or omitting the stiffness contributions of continuous RC slabs in the calculations lead to a consideration of the building that is much weaker than it is in reality. On the other hand, Calculation 1 and Calculation 2 underestimate the front wall damage. This shows that both original LTSM and the LTSM with E/G=9.5 account for a much higher stiffness than that the building specimen has in reality. It should also be highlighted that

the predictions made by Calculations 1 and 2 are not safe from the aspects of intervention planning and damage prevention.

Table 6.4. Analytical results of Test 3.

Calculation	Δ/L	Ɛbmax (%)	Ɛdmax (%)	Damage Class obtained by LTSM	Actual Damage Class obtained by tests [Front Wall (DMS aspect)]
1	0,001753	0,1973	0,1465	Moderate	Severe
2	0,001753	0,0613	0,1664	Moderate	
3	0,001753	0,8909	0,0454	Very Severe	
4	0,001753	1,1343	0,0099	Very Severe	
5	0,001753	0,7084	0,0719	Very Severe	
6	0,001753	1,0759	0,0184	Very Severe	

6.2. Results For Joist Floor Specimen (Test 4)

6.2.1. Test 4

The maximum crack width of the front wall was about 36 mm (72 mm in full size building). Based on this, actual damage for this specimen was very severe. As seen in Table 6.5, damage classes calculated by LTSM using Calculations 3, 5 and 6 are in line with the severity of the front wall damage. Calculation 4 is not applicable for joist floor specimen test, because this calculation considers the contribution of floor slabs only. Calculation 1 and Calculation 2 underestimate the damage class. This result should be highlighted. Although joist floor specimen has a target typology for the classical applications of LSTM (i.e. Calculations 1 and 2) because of the presence of a flexible diaphragm, Calculations 1 and 2 cannot predict its damage class accurately.

Table 6.5. Analytical results of Test 4.

Calculation	Δ/L	Ɛbmax (%)	Ɛdmax (%)	Damage Class obtained by LTSM	Actual Damage Class obtained by tests [Front Wall (DMS aspect)]
1	0,002484	0,2795	0,2076	Moderate	Very Severe
2	0,002484	0,0869	0,2357	Moderate	
3	0,002484	1,5245	0,0261	Very Severe	
4	0,002484	-	-	-	
5	0,002484	1,0038	0,1020	Very Severe	
6	0,002484	1,5245	0,0261	Very Severe	

6.3. Results For Combined Specimen (Test 5)

6.3.1. Test 5

The maximum crack width of the front wall was 4.5 mm (9 mm in full size building) and 0 mm (0 mm in full size building) on the back wall. Recall that, this specimen consisted of two different walls: front wall was the perforated (5-openings) wall, and the back wall was the blind (zero opening) wall. Based on this, actual damage class for the front wall of this specimen was moderate. As seen in Table 6.6, damage classes calculated by LTSM using Calculations 1 and 2 underestimate the front wall damage. Calculations 3, 4, 5 and 6 overestimate the front wall damage. As stated in Chapter 5, E/G ratio was taken as 12.5 for Calculations 1 and 2.

Table 6.6. Analytical results of Test 5.

Calculation	Δ/L	Ɛbmax (%)	Ɛdmax (%)	Damage Class obtained by LTSM	Actual Damage Class obtained by tests [Front Wall (DMS aspect)]
1	0,001346	0,0362	0,1293	Slight	Moderate
2	0,001346	0,0362	0,1293	Slight	
3	0,001346	0,8489	0,0108	Very Severe	
4	0,001346	0,8709	0,0076	Very Severe	
5	0,001346	0,5737	0,0509	Very Severe	
6	0,001346	0,8967	0,0038	Very Severe	

6.4. Discussion

In this study, except for Calculation 2, results of all analytical methods for all specimens showed that the maximum bending strain (ε_{bmax}) was larger than the maximum diagonal (shear) strain (ε_{dmax}). In other words, bending strains were more critical. Although the bending strains of all specimens were more critical than diagonal (shear) strains, only the Joist floor specimen failed in pure bending mode. This difference in the response of the joist floor specimen was because of the floor type. This result shows that beam analogy is not capable of representing the governing damage mode (except for

joist floor specimen) of the building specimens because of not considering the function of RC continuous floors of suppressing the transfer of the settlement effects (i.e. distortions and damages) from the first to the second story. Although the Calculations 3, 4, 5 and 6 consider the contribution of slabs to the building stiffness, the ultimate damage pattern cannot be predicted. The following paragraphs are devoted to the summary/analyses of the prediction success of each calculation method.

Prediction of Test 1: It was obvious that LTSM with different stiffness relations (Calculations 3, 4, 5 and 6) can estimate the damage class, while classical one (Calculation 1) and Calculation 2 underestimate. This is because of the overestimation of the building stiffness in these methods.

Predictions of Test 2 and Test 3: None of the methods could predict damage classes correctly. While Calculation 1 and 2 underestimate the damage classes; Calculations 3, 4, 5 and 6 overestimate.

Prediction of Test 4: Although the Joist floor specimen offers a structural typology that fits in a great extent to the building configurations adopted in the development of the beam analogy by Burland and Wroth (1974) the classical LTSM (Calculation 1) could not predict the damage class of this specimen. The other methods which had different stiffness modifications for LTSM (Calculations 3, 5 and 6) could estimate the damage class.

Prediction of Test 5: While the Calculation 2 underestimate the damage class of the front wall (perforated wall) of the combined specimen, Calculations 3, 4, 5 and 6 overestimate. Unlike the preceding predictions, the classical LTSM (Calculation 1) can estimate the damage class of this specimen.

Comparison of damage categories were made by using both test results and LTSM results. It was seen that Calculations 3, 5 and 6 were more successful to determine the damage category in general. However, Calculation 2 produced worst results in terms of damage category.

CHAPTER 7

CONCLUSION

In this study, to examine the behavior of historical masonry walls subjected to simulated tunneling-induced ground settlement, large scale experimental tests were conducted. In total, three different building wall specimens (reference, joist floor and combined) that have different floor types and opening ratios were constructed in ½ scale and tested in the experimental campaign. While two of these specimens had continuous RC stiff slabs, one had RC joists as the flooring system. Test results show that:

- The settlement response of the specimens is affected by the floor type in a great extent. The presence of RC continuous floors results in a serious modification of applied settlement profile (gapping in the tests). This can be explained through a specific mechanism. It is thought that RC continuous floors are working like a so-called "tension cord" with high axial stiffness at the top of the masonry walls at both stories. Unless the bond between the masonry wall and RC continuous floor is broken, the so-called cords keep working and lead to having the specimens being suspended against the downward settlement displacements. On the other hand, loading RC floors with additional loads makes the masonry-RC floor bond much stronger due to increased normal compressive stresses and friction. Joist floor specimen that has no continuous RC floor behaved like a beam and showed a much higher conformity to the applied settlements.
- The effect of window openings is examined using reference, joist floor and combined specimens. Regardless the floor type, it is seen that as the number of the openings increases, a more distributed damage pattern is obtained. This is because of the fact that sharp corners of the slender piers around the openings lead to stress concentrations.

LTSM is used with different stiffness relations and final damage class of each wall is predicted. Analytical calculations are capable of showing increasing or decreasing

damage vulnerability of the specimens for achieved deflection ratio values, however they can make coarse predictions for most of the wall configurations. The best predictions were made for the joist floor specimen because this specimen fits to the target structural typology of the used beam methods. Underestimation of the damage class of the specimens even by the classical LTSM reveals an important issue from the damage prevention and structural safety aspects during tunneling excavations. In contrary to this finding, especially the classical LTSM used to be known as quite conservative in the practical applications.

REFERENCES

Amorosi, A., Boldini, D., De Felice, G., Malena, M., & Sebastianelli, M. 2014. "Tunnelling-induced deformation and damage on historical masonry structures." Géotechnique, 64, 118-130. doi: 10.1680/geot.13.p.032

Ates, A.O., Khoshkholghi, S., Tore, E., Marasli, M., Ilki, A. 2019. "Sprayed glass fiber-reinforced mortar with or without basalt textile reinforcement for jacketing of low-strength concrete prisms." ASCE J. Compos. Constr. 23(2), 04019003.

Boscardin, M. 1980. "Building response to excavation-induced ground movements" (Ph.D. Thesis). University of Illinois at Urbana-Champaign, Champaign, IL.

Boscardin, M. D., & Cording, E. J. 1989. "Building response to excavation-induced."

Burd, H. J., Houlsby, G. T., Augarde, C. E., & Liu, G. 2000. "Modelling tunnelling-induced settlement of masonry buildings." Proceedings of the Institution of Civil Engineers - Geotechnical Engineering, 143, 17-29. doi: 10.1680/geng.2000.143.1.17

Burhouse, P. 1969. "Composite action between brick panel walls and their supporting beams." Proceedings of the Institution of Civil Engineers, 43, 175-194. doi: 10.1680/iicep.1969.7381

Burland, J., Mair, R., & Standing, J. 2004. "Ground performance and building response due to tunnelling." In R. J. Jardine, D. M. Potts, and K. G. Higgins (Eds.), Advances in Geotechnical Engineering. Institution of Civil Engineers, 1, 291-342.

Burland, J., & Wroth, C. 1974. "Settlement of buildings and associated damage." Proceedings of conference on settlement of structures, Cambridge.

Burland, J., Broms, B., & de Mello, V. 1977. “Behavior of foundations and structures.” 9th International Conference on Soil Mechanics and Foundation Engineering, Tokyo.

Comodromos, E. M., Papadopoulou, M. C., & Konstantinidis, G. K. 2014. “Numerical assessment of subsidence and adjacent building movements induced by TBM-EPB tunnelling.” Journal of Geotechnical and Geoenvironmental Engineering, 140, 04014061.
doi: 10.1061/(asce)gt.1943-5606.0001166

Dalgic, K.D, Hendriks, M.A.N, Ilki, A. 2017. “Building response to tunnelling- and excavation-induced ground movements: using transfer functions to review the limiting tensile strain method.” Structure and Infrastructure Engineering, 14, 766-779.
doi: 10.1080/15732479.2017.1360364

Dalgic, K.D, Gulen, D.B, Acikgöz, S., Burd, H., Hendriks, M.A.N, Giardina, G., Ilki, A. 2021. “Large scale experimental settlement tests to evaluate structural models for tunnelling-induced damage analysis.” Lecture Notes in Civil Engineering, 126.
doi: 10.1007/978-3-030-64518-2_20

Finno, R.J, Voss Jr., F.T, Rossow, E., Blackburn, J.T. 2005. “Evaluating damage potential in buildings affected by excavations”. ASCE, 10, 1199.
doi: 10.1061/(ASCE)1090-0241

Giardina, G., Marini, A., Hendriks, M. A. N., Rots, J. G., Rizzardini, F., & Giuriani, E. 2012. “Experimental analysis of a masonry façade subject to tunnelling-induced settlement.” Engineering Structures, 45, 421-434.
doi: 10.1016/j.engstruct.2012.06.042

Giardina, G., van de Graaf, A. V., Hendriks, M. A. N., Rots, J. G., & Marini, A. 2013. “Numerical analysis of a masonry façade subject to tunnelling-induced settlements.” Engineering Structures, 54, 234-247.

doi: 10.1016/j.engstruct.2013.03.055

Giardina, G., Hendriks, M. A. N., & Rots, J. G. 2015. “Sensitivity study on tunnelling induced damage to a masonry façade.” Engineering Structures, 89, 111-129. doi: 10.1016/j.engstruct.2015.01.042

Giardina, G., DeJong, M.J., Chalmers, B., Ormond, B., Mair, R.J. 2018. A comparison of current analytical methods for predicting soil-structure interaction due to tunnelling”. Tunnelling and Underground Space Technology, 79, 319-335. doi: 10.1016/j.tust.2018.04.013

Goh, K. H., & Mair, R. J. 2014. “Response of framed buildings to excavation-induced movements.” Soils and Foundations, 54, 250-268. doi: 10.1016/j.sandf.2014.04.002

Gulen, D. B, Acikgoz, S., Burd, H. 2019. “FBG Sensor and DIC Instrumentation Plan.” (REPORT)

Hsieh, P. G., & Ou, C. Y. 1998. Shape of ground surface settlement profile caused by excavation. Canadian Geotechnical Journal, 35, 1004–1017. doi:10.1139/cgj-35-6-1004

Ilki, A., et al. 2007. “Seismic safety of a historical row house complex built during Ottoman period.” Proc., 9th Canadian Conf. on Earthquake Engineering CD-ROM, Ottawa, Canada, 830–839.

Ispir, M. 2010. “A comprehensive experimental research on the behavior of historical brick masonry walls of 19th century buildings”. PhD Thesis.

Ispir, M., Ilki, A. 2013. “Behavior of historical unreinforced brick masonry walls under monotonic and cyclic compression.” Arab. J. Sci. Eng. 38(8), 1993–2007 doi: 10.1007/s13369-013-0567-4

Jenck, O., & Dias, D. 2004. “3-D finite difference analysis of the interaction between concrete building and shallow tunnelling.” Geotechnique, 54, 519-528. doi:10.1680/geot.54.8.519.52011

Laefer, D.F., Hong, L.T., Erkal, A., Long, J.H., Cording, E.J. 2011. “Manufacturing, assembly, and testing of scaled, historic masonry for one-gravity, pseudo-static, soil-structure experiments.” Constr. Build. Mater. 25(12), 4362–4373

Little, M. 1969. “Discussion-Session 6. Proceedings of Symposium on Design for movement in buildings.” London.

Mainstone, R. 1974. “Discussions, Session 5. Proceedings of conference on settlement of structures.” Cambridge.

Mainstone, R., & Weeks, G. 1970. “The influence of a bounding frame on the racking stiffness and strengths of brick walls.” SIBMAC Proc. 165-171

Mair, R., Taylor, R., & Burland, J. 1996. “Prediction of ground movements and assessment of risk of building damage due to bored tunnelling.” Fourth International Symposium of International Conference of Geotechnical Aspects of on Underground Construction in Soft Ground.

Melis, M., Rodriguez Ortiz, J. 2001. “Consideration of the stiffness of buildings in the estimation of subsidence damage by EPB tunnelling in the Madrid subway.” Response of Buildings to Excavation Induced Ground Movements Conference, London.

Moncarz, P.D., & Krawinkler, H. 1981. “Theory and application of experimental model analysis in earthquake engineering.” The John A. Blume Earthquake Engineering Center, Department of Civil and Environmental Engineering, Stanford University.

Mroueh, H., & Shahrour, I. 2003. “A full 3-D finite element analysis of tunneling–adjacent structures interaction.” Computers and Geotechnics, 30, 245-253.

doi:10.1016/s0266-352x(02)00047-2

Netzel, H. 2009. “Building response due to ground movements.” Delft University of Technology, Delft.

Peck, R. 1969. Deep excavations and tunneling in soft ground. Proceedings of the 7th international conference on soil mechanics and foundation engineering, Mexico.

Peck, R., Deere, D., & Capacete, J. 1956. “Discussion on paper by Skempton and MacDonald 'Allowable settlements of buildings'.” Proc Instn Civ Engrs, 5, 778.

Polshin, D., & Tokar, R. 1957. “Maximum allowable non-uniform settlement of structures.” Proceedings of the fourth international conference on soil mechanics and foundation engineering, London.

Potts, D. M., & Addenbrooke, T. I. 1997. “A structure's influence on tunnelling-induced ground movements.” Proceedings of the Institution of Civil Engineers - Geotechnical Engineering, 125, 109-125.
doi: 10.1680/igeng.1997.29233

Ritter, S., Giardina, G., DeJong, M.J., Mair, R.J. 2017. “Centrifuge modelling of building response to tunnel excavation.” Int. J. Phys. Model. Geotech., 1–16. https://doi.org/10.1680/jphmg.16.00053

Skempton, A. W., & Macdonald, D. H. 1956. “The allowable settlements of buildings.” Proceedings of the Institution of Civil Engineers, 5, 727-768.
doi:10.1680/ipeds.1956.12202

Son, M. 2003. “The response of buildings to excavation-induced ground movements.” University of Illinois at Urbana-Champaign, Champaign, IL

Son, M., & Cording, E. J. 2005. “Estimation of building damage due to excavation-induced ground movements.” Journal of Geotechnical and Geoenvironmental Engineering, 131, 162-177.

doi: 10.1061/(asce)1090-0241(2005)131:2(162)

Son, M., & Cording, E. J. 2007. “Evaluation of building stiffness for building response analysis to excavation-induced ground movements.” Journal of Geotechnical and Geoenvironmental Engineering, 133, 995-1002. doi: 10.1061/(asce)1090-0241(2007)133:8(995)